Distribution of Hcn in Titan's Upper Atmosphere from Cassini/Vims Observations At 3 Microns

A. Adriani, B.M. Dinelli, M. López-Puertas, M. García-Comas, M.L. Moriconi, E. d'Aversa, B. Funke, A. Coradini

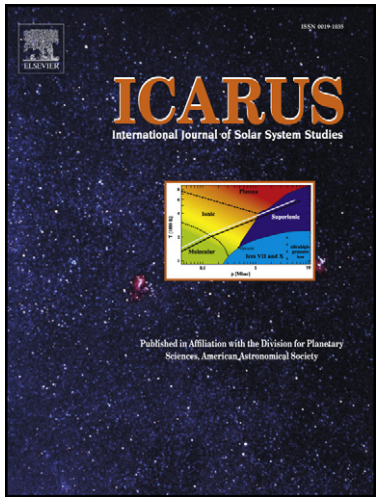

Distribution of Hcn in Titan's Upper Atmosphere from Cassini/Vims Observations At 3 Microns

A. Adriani, B.M. Dinelli, M. López-Puertas, M. García-Comas, M.L. Moriconi, E. D'Aversa, B. Funke, A. Coradini

PII: S0019-1035(11)00151-5
DOI: 10.1016/j.icarus.2011.04.016
Reference: YICAR 9793

To appear in: *Icarus*

Received Date: 3 December 2010
Revised Date: 18 April 2011
Accepted Date: 21 April 2011

Please cite this article as: Adriani, A., Dinelli, B.M., López-Puertas, M., García-Comas, M., Moriconi, M.L., D'Aversa, E., Funke, B., Coradini, A., Distribution of Hcn in Titan's Upper Atmosphere from Cassini/Vims Observations At 3 Microns, *Icarus* (2011), doi: 10.1016/j.icarus.2011.04.016

DISTRIBUTION OF HCN IN TITAN'S UPPER ATMOSPHERE FROM CASSINI/VIMS OBSERVATIONS AT 3 MICRONS

A. Adriani[1], B. M. Dinelli[2], M. López-Puertas[3], M. García-Comas[3], M. L. Moriconi[4], E. D'Aversa[1], B. Funke[3], A. Coradini[1]

[1] *IFSI-INAF,*

Via Fosso del Cavaliere 100, I-00133, Rome, Italy

[2]*ISAC-CNR,*

Via Gobetti 101, I-40129, Bologna, Italy

[3]*Instituto de Astrofísica de Andalucía, CSIC,*

Camino Bajo Huétor, 50, E-18008 Granada (Spain)

[4]*ISAC-CNR,*

Via Fosso del Cavaliere 100, I-00133, Rome, Italy

Number of pages: 57

Number of tables: 4

Number of figures: 16

Proposed Running Head:

HCN Titan Upper Atmosphere

Please send Editorial Correspondence to:

Alberto Adriani

Institute of Physics of Interplanetary Space

Via Fosso del Cavaliere, 100

00133, Rome

Italy

Email: alberto.adriani@ifsi-roma.inaf.it

Phone: +39 0645488365

Fax: +39 0645488383

Abstract

Cassini/VIMS limb observations have been used to retrieve vertical profiles of hydrogen cyanide (HCN) from its 3 μm emission in the region from 600 to 1100 km altitude at daytime. While the daytime emission is large up to about 1100 km, it vanishes at nighttime at very low altitudes, suggesting that the daytime emission originates under non-LTE conditions. The spectrally integrated radiances around 3.0 μm shows a monotonically decrease with tangent altitude, and a slight increase with solar zenith angle in the 40º-80º interval around 800 km.

A sophisticated non-LTE model of HCN energy levels has been developed in order to retrieve the HCN abundance. The population of the HCN $00^0 1$ energy level, that contributes mostly to the 3.0 μm limb radiance, has been shown to change significantly with the solar zenith angle (SZA) and HCN abundance. Also its population varies with the collisional rate coefficients, whose uncertainties induced errors in the retrieved HCN of about 10% at 600-800 km and about 5% above. HCN concentrations have been retrieved from a set of spectra profiles, covering a wide range of latitudes and solar zenith angles, by applying a line-by-line inversion code. The results show a significant atmospheric variability above ~800 km with larger values for weaker solar illumination. The HCN shows a very

good correlation with solar zenith angles, irrespective of latitude and local time, suggesting that HCN at these high altitudes is in or close to photochemical equilibrium. A comparison with UVS and UVIS measurements show that these are close to the lower limit (smaller SZAs) of the VIMS observations above 750 km. However, they are in reasonable agreement when combining the rather large UV measurement errors and the atmospheric variability observed in VIMS. A comparison of the mean profile derived here with the widely used profile reported by Yelle and Griffith (2003) shows a good agreement for altitudes ranging from 850 to 1050 km, while below these altitudes our result exhibits higher concentrations.

.

Keywords: Atmospheres, composition; Infrared observations; Radiative transfer; Titan, atmosphere.

1 Introduction

To date, the Titan atmosphere in the altitude range between 600 and 1100 km has been poorly investigated. This region is very important because it acts as an incubator where the photochemical and nucleation processes lead to the production of heavy molecules that, through sedimentation and coagulation, originate the lower atmosphere aerosols.

The hydrogen cyanide (HCN) is produced by photochemical reactions in the mesosphere and thermosphere of Titan (Banaskiewicz et al., 2000; Wilson and Atreya, 2004). This nitrile is thought to play an important role in the chemistry of those regions and in determining the thermal structure of Titan's thermosphere (Yelle, 1991; Kranospolsky, 2010). At present, the region above 900 km is thought to be in radiative equilibrium, maintained by the balance between EUV/UV solar heating and the HCN rotational cooling (Yelle, 1991). Since the HCN distribution in this region is poorly known, new measurements of this species will improve our understanding of the chemical processes and thermal structure of the thermosphere.

In the past years, HCN has been detected in the Titan's atmosphere in the infrared, by the IRIS instrument (Hanel et al., 1981; Coustenis and Bèzard, 1995), and in the ultraviolet, by the UVS (Strobel and Shemansky, 1982; Vervack et al., 2004), both on board Voyager 1. Observations in the thermal infrared were

performed by the Infrared Space Observatory (ISO) in 1997, revealing the HCN spectral emission near 700 cm^{-1} (Coustenis et al., 2003). HCN has also been measured from ground-based observations in the millimeter range, using the IRAM 30-m telescope in Spain (Marten et al., 2002), and in its characteristic fluorescence emission near 3.0 μm by using NIRSPEC at the Keck II telescope in Mauna Kea (Geballe et al., 2003; Yelle and Griffith, 2003; Kim et al., 2005).

In a first analysis of the 3.0 μm ground observations, Geballe et al. (2003) derived a HCN concentration near the mesopause about three orders of magnitude larger than photochemical models predictions. The same observations were analyzed later by Yelle and Griffith (2003), demonstrating that the observed emission comes actually from much lower altitudes (around 1 mb, ~200 km) and that it is insensitive to the HCN concentration in the upper mesosphere and thermosphere. Kim et al. (2005) further re-analyzed those measurements and found similar conclusions to those obtained by Yelle and Griffith. Hence, these ground-based measurements, taken in the same spectral region as VIMS but in the nadir instead of the limb, are sensitive to the HCN abundance in the upper stratosphere/lower mesosphere region only.

More recently, the Cassini mission has provided a more extensive dataset of HCN in Titan's atmosphere. On a first

instance, the Composite Infra-Red Spectrometer (CIRS) has taken nadir and limb observations between July 2004 and January 2007 providing HCN concentrations from the surface up to about 500 km covering almost all latitudes (Flasar et al., 2005; Teanby et al., 2007). The retrieved abundances might, however, be affected by systematic errors due to the uncertainties in the retrieved temperatures (Teanby et al., 2008). Another instrument on Cassini, the Ion and Neutral Mass Spectrometer (INMS), has measured HCN in the thermosphere. A mean value of the HCN Volume Mixing Ratio (VMR) in the range of 1000 to 1100 km has been obtained from 16 Titan encounters from 2004 to 2008 (Waite et al., 2008). Although the precision of this value is high, it is affected by a 20% systematic calibration uncertainty. Furthermore, the C_2-species C_2H_2, C_2H_4, C_2H_6, and the primary nitrile HCN, have a significant overlap at the INMS mass resolution and are therefore subjected to an additional uncertainty. In addition to those instruments, HCN abundances have also been retrieved from UVIS (Ultraviolet Imaging Spectrometer) measurements during the two stellar occultations of Shaula (λ Sco) and Spica (α Vir), located in the southern and northern hemisphere, respectively, during the T_B flyby (Shemansky et al., 2005; Liang et al, 2007). The UV absorption spectrum of Titan's upper atmosphere is sensitive to six species: CH_4, C_2H_2, C_2H_4, C_2H_6, HCN, and C_4H_2, but their absorption

features are heavily overlapped. The HCN number densities derived from the Spica occultation are reported with systematic uncertainties as large as 100%.

We report here the measurements of HCN concentrations in Titan's upper atmosphere retrieved from the Cassini Visual Infrared Mapping Spectrometer (VIMS) limb observations in the 3.0 μm region. These observations contain information on the daytime HCN abundance in the 600-1100 km altitude range and are thus very important because: a) they extent the altitude range of HCN measurements taken previously in this spectral region by ground-based measurements; b) they the fill the gap between CIRS measurements below 500 km and the INMS measurements above 1000 km; and c) they are more accurate than the UVIS measurements taken in the same atmospheric region.

The paper is organized as follows: in Sec. 2 we describe the spectral radiance measurements and its major features. Sec. 3 describes the non-LTE modeling required to invert the daytime HCN 3.0 μm non-LTE emission. The inversion of the spectra into HCN vertical profiles is described in Sec. 4. The retrieved HCN abundances and a comparison with previous measurements are discussed in Sec. 5. The major conclusions are summarized in Sec. 6.

2 Observations

2.1 Data description

VIMS is a multi-channel mapping spectrometer on board Cassini working in the 0.35-5.1 μm wavelength range (Brown et al., 2004). In this work we are focused in the infrared region, around 3 μm, where HCN has its stronger vibrational bands. In this spectral interval, VIMS measures in adjacent channels with an average spectral sampling of 16 nm (~18 cm^{-1}). It takes hyper-spectral images of Titan, covering a few thousands kilometers of its atmosphere, with a pixel field of view of 0.5 by 0.5 mrad. The ensemble of these images is organized in cubes with two spatial dimensions and a third one in the spectral domain (Brown et al., 2004).

In order to explore the different areas of the Saturn system, the Cassini mission was designed to have many close encounters with Titan. Though VIMS had observed Titan's atmosphere during these encounters and from different perspectives, suitable conditions for observing its upper atmosphere and ionosphere have not been frequent. The first necessary condition is to have images with long integration times, so the limb emission from these thin high regions have large enough signal to noise (S/N) ratios. In this sense, we have chosen only those observations with a high degree of saturation in the visual channel at the Titan's surface, a proxy for long

exposure time. The phase angle is also crucial as stray-light effects can modify the original signal at high phase angles. So far, algorithms able to remove those distortions are not available. We then selected the observations with phase angles lower than 90°. The cubes analyzed in this study, together with their exposure times, mean vertical resolutions, and phase angles, are listed in Table 1. As an example Figure 1 shows the radiances measured by VIMS for cube 9485 in the 3.064 μm channel (left panel) and in the 2.900 μm channel (right panel). In the figure Titan is white-masked to emphasize the atmospheric emission. The data have been calibrated geometrically, using *ad hoc* algorithms based on NAIF-SPICE tools (Acton et al., 1996), and radiometrically, using the RC17 calibration pipeline (McCord et al., 2004; Filacchione, 2006; Filacchione et al., 2007). The typical instrument noise error of VIMS in the 3.0 μm region is about 3×10^{-8} W m^{-2} nm^{-1} sr^{-1}. Regarding the spectral calibration, VIMS IR wavelength values vary almost linearly with the band number, following the expression $\lambda = 0.01668\times111xB - 0.7381$ μm, where B=96-351 for the IR channel. Only one clear pattern deviation, although small, from that linear fit has been observed (Cruikshank et al., 2010) but it is outside of our region of interest.

Figure 1

Titan atmosphere was studied extracting from VIMS cubes the spectra corresponding to the pixels lying outside Titan's disk. The spectra were divided into sets (collections) each corresponding to the pixels encountered by an ideal straight line perpendicular to Titan's surface. The extracted pixels belonging to individual collections have been labeled according to their 'tangent altitude' that is the distance of the observed pixel from the surface of Titan and the geo-location of the origin of the ideal vertical line. As an example of the extraction method, in the left panel of figure 1 we have designed the lines that denote the latitudes on Titan surface and the vertical lines used to extract the corresponding collections of spectra. Various collections of spectra in the altitude range of 400-1100 km have been extracted from each cube, preserving, as far as possible, the verticality of each profile. An example of the spectral intensities collected in correspondence of one of those collections is shown in Figure 2, where we report in different colors the spectrum of Titan's atmosphere relative to different tangent altitudes. . The vertical resolution of the extracted spectra was calculated as the mean absolute difference of the tangent altitudes at the upper and lower corners of the pixels. The Solar Zenith Angle (SZA) relative to the individual spectra was calculated by applying the Euler law of the cosines to the spherical triangle with vertices at the appropriate geographical pole, the sub-solar point, and at the

intercept of the normal to the surface from each pixel's tangent altitude. In this study 33 spectral collections have been analyzed covering mainly the southern hemisphere (see Table 1). Cubes at other locations and times did not fulfill the conditions for S/N and phase angles discussed above.

Figure 2

2.2 HCN emission

Figure 1 shows the emission from a typical cube V1567269485 at two different wavelengths: at 3.064 μm (left), where both the atmospheric molecular emission and the atmospheric scattering contribute (see Figure 2), and at 2.900 μm (right), where the scattering is the major component. By inspection of the atmospheric limb glow in VIMS images in Figure 1 (compare left and right panels) we can see that the lowest part of Titan's daylight atmosphere, approximately below 400 km, is dominated by the aerosol scattering. This contribution appears to be significant up to 3.6 μm (Figure 2). Above 500 km, the scattering contribution becomes impossible to distinguish from the instrumental noise level in the 3 μm wavelength region (see right panel of Figure 1 and Figure 2). For this reason we assumed negligible its contribution. Since our study is focused on the atmospheric emission of the HCN molecule, we are then limited to analyze data coming from altitudes above 500 km.

Figure 2 shows a typical sequence of VIMS spectra in the 2.8-3.7 μm region. The collection of spectra was extracted from cube V1563524168 taken at latitude 70ºS and with SZA=60.8º. The figure shows the sequence of spectra from 275 to 1062 km. Even if the spectral resolution of VIMS is moderate (about 16 nm FWHM), two emission bands one at 3 μm mainly due to HCN and one at 3.3 μm, mainly due to CH_4, are clearly visible at all altitudes. In this work, we analyze the spectral feature centered near 3.0 μm, while the study of the emission in the 3.2-3.5 μm spectral range is described in García-Comas et al. (2010).

The atmospheric emission near 3 μm is mainly due to the ν_3 fundamental band of HCN. However, nearly overlapped to the HCN bands but slightly (~25 nm) red-shifted, C_2H_2 also contributes significantly, particularly at altitudes below 800-900 km. The emission of these two molecules appears overlapped at the spectral resolution of VIMS; however at the pressures and temperatures expected for Titan's mesosphere and thermosphere the single emission lines of the two molecules do not overlap, so that they can be considered independent. An estimation performed with the non-LTE model for HCN described in Sec. 3 and a simple calculation of the C_2H_2 excitation temperature showed that the C_2H_2 contribution at a tangent height of 650 km is about 30% and decreases rapidly to 20% at 750 km, 10% at 850 km, 8% at 950 km, and 6% at 1050 km. Recently, Seo et al.

(2009) have identified in Titan's spectrum, observed at high resolution, two bands of C_2H_6, one centred at 2.94 and one at 3.07 μm. Both are very weak bands (20 times weaker than the main C_2H_6 band ν_7). The 3.07 μm band lays in the same spectral region of the HCN and C_2H_2 emission considered here. However, the 2.94 μm band, that lays outside the HCN spectral range, was not identified into Titan's examined spectra. Therefore we expect no significant contribution of the 3.07 μm band of C_2H_6 to the HCN spectral signature. The fact that the 3.0 μm emission disappears at night (see Figure 1) demonstrates that it is emitted under non-LTE conditions during daytime, when it is mainly excited by the solar absorption at the same wavelength of emission. More details on the excitation processes are given in Sec. 3.

Figure 3 shows a contour plot of the measured radiances, integrated over the spectral interval between 2.97 and 3.10 μm, as a function of tangent altitude and solar zenith angle. A cut of this plot at the lower SZAs shows that the radiance decreases slightly with altitude up to about 800 km and then decreases more rapidly at higher tangent altitudes. This, in turn suggests that the HCN abundance does not decrease monotonically with altitude, i.e., pressure below about 800 km.

Figure 3

We can also appreciate that the variation of the radiance profiles for SZA ranging from 40 to 70-80 is small at almost all altitudes. Given that the excitation temperatures for this range of SZAs changes only slightly (see Sec. 3 and Figure 7), it then hints at a small variation of HCN with SZA. It is however very interesting to note that at tangent height above around 800 km, the radiance is constant or slightly increases with SZA up to SZA=80º. As SZA increases, absorption from solar radiation diminishes and hence vibrational temperatures decrease (see Figure 7). The larger radiance at high SZAs (limited below 80º) then suggests higher HCN abundances at high SZA. This aspect is discussed in more detail and quantitatively in Sec. 5.

The radiances fall off at SZA larger than 80º is mainly due to the weaker absorption of solar radiation at those tangent heights. The solar flux for the slant paths is absorbed at higher altitudes and less photons reach the lower atmospheric regions (see Figure 7). We should note, however, that even for SZA as large as 100º, the solar radiation still reaches the atmosphere even at altitudes as low as 500 km (see Figure 7). In the next section we describe the non-LTE modeling necessary for inverting those radiances in HCN abundances.

3 Non-LTE modeling

3.1 The model

The HCN 3.0 μm emission in Titan atmosphere was first reported by Geballe et al. (2003) from ground based measurements. They also developed a simple non-LTE model to derive the HCN concentration in Titan's middle atmosphere from their measurements. These data were revised shortly afterwards by Yelle and Griffith (2003) reporting an improved non-LTE modeling, constraining the collisional relaxation of the HCN (00^01) level (ν_3 H-C bond stretching mode), which is the major contributor to the nadir Titan radiance near 3.0 μm, and revising significantly the HCN middle atmosphere abundance. Kim et al. (2005) lately revised the study of Geballe et al. (2003) and found a range of HCN mixing ratio profiles that are consistent with the HCN abundance derived by Yelle and Griffith (2003).

Those previous models were developed for analyzing the HCN 3.0 μm emission measured in the nadir direction. The limb measurements taken by VIMS require, however, a more detailed non-LTE model since weaker HCN bands might contribute significantly to the emission at higher limb altitudes, given that the strongest ($00^01 \rightarrow 000$) band becomes optically thick in the limb at tangent heights above around 700 km.

We have calculated the HCN vibrational temperatures by adapting the Generic RAdiative traNsfer AnD non-LTE population Algorithm (GRANADA), originally developed for the Earth's atmosphere (Funke et al., 2002), to the Titan's atmosphere. Briefly, the model uses a generalized scheme for the inclusion of the radiative and collisional processes affecting the population of the vibrational levels of the specified molecule(s). It has many "user-defined" features including, among others, the states and transitions to be considered, the altitude range, the iteration strategy for solving the steady state and the radiative transfer equations, and the non-LTE (collisional and radiative) processes to be included. The model is capable of calculating rotational and spin-orbit non-LTE populations, although, for this study, we considered rotational LTE. Local thermodynamic equilibrium is commonly assumed for the rotational levels in the ground vibrational state of HCN (see, e.g., Yelle, 1991). The extension of LTE to the rotational levels in the vibrational excited states is justified because they are mainly excited by the absorption of solar radiation that excites all rotational levels in a very similar manner. Radiative transfer can be performed either line-by-line or by using line independent methods (i.e. histogramming of involved lines). All radiative transfer calculations are based on the Karlsruhe Optimized and Precise Radiative Transfer Algorithm (KOPRA) (Stiller et al., 2002).

The line-by-line option was used in this study for all transition treated with radiative transfer. The inversion of the system of multilevel steady state equations can be performed by either using the Lambda-iteration or the Curtis matrix formalisms. The Curtis matrix formalism was used here.

We have computed the populations of the HCN energy levels listed in Table 2 and Table 3 and the collisional processes described in Table 4. The strongest $01^{1}0 \rightarrow 000$, $00^{0}1 \rightarrow 000$, $01^{1}1 \rightarrow 000$, $01^{1}1 \rightarrow 01^{1}0$, and $00^{0}2 \rightarrow 000$ bands have been treated with radiative transfer by using the Curtis matrix method in the whole altitude range of 0-1500 km. A line-by-line calculation of the upwelling tropospheric flux given by the temperature of the lower boundary (Titan's surface) and the solar flux at the top of the atmosphere were assumed for all bands. The spectroscopic data for HCN were taken from the HITRAN compilation, 2008 edition. Other bands not included in the compilation, as the $01^{1}1 \rightarrow 000$, $01^{1}1 \rightarrow 01^{1}0$, $00^{0}2 \rightarrow 000$, and $00^{0}2 \rightarrow 00^{0}1$ transitions, were taken from the HCN compilation of Harris et al. (2002). Solar fluxes in the IR and near IR have been taken from the SOLAR2000 compilation (Tobiska et al., 2000).

About the collisional processes (see Table 4), process 1 represents the collisional de-excitation of the HCN ν_2 levels in

collisions with the major atmospheric constituent in Titan atmosphere, N_2. The rate coefficient has been taken from the recent measurements of Srinivasan et al. (2008) for collisions with Kr, scaled by a factor of 0.3 to account for the $k_2(N_2)/k_2(Kr)$ ratio, as reported by Arnold and Smith (1981).

Process 2 accounts for the redistribution of the vibrational energy of HCN among the ν_1 and ν_2 modes. The relaxation of one ν_1 quanta has enough energy to excite up to three ν_2 vibrations. The rate for this process has also been taken from Srinivasan et al. (2008) and corrected for the $k_2(N_2)/k_2(Kr)$ ratio as reported by Arnold and Smith (1981).

Process 3 accounts for the relaxation of the HCN ν_3 mode, which is the most important process for the analysis of the VIMS measurements reported here. Hasting et al. (1983) have demonstrated that the relaxation of the ν_3 mode takes place through a re-arrangement of the ν_3 vibrational energy into the ν_1 and ν_2 modes (the relaxation of one ν_3 quantum excites one ν_1 and two ν_2 quanta) and then relax to lower energetic levels by the de-activation of the ν_1 and ν_2 modes. Since the relaxation of the ν_2 mode is faster than that of ν_1, the relaxation of the $\nu3$ mode takes place ultimately through collisions where one ν_2 quanta is involved. The quenching rate coefficient of the ν_3 mode has been measured by Hasting et al. (1983) reporting a value of

$2.6x10^{-14}$ cm^3s^{-1} for the relaxation of the HCN (00^02) at room temperature. The quenching rates usually decrease with temperature and hence the value at the typical Titan temperatures should be smaller. Yelle and Griffith (2003) showed in their analysis of the ground-based HCN 3.0 μm nadir measurements that a value of $2x10^{-15}$ cm^3s^{-1} gives the best fit between measurements and model simulations. Based on these arguments we have taken in the nominal model the value suggested by Yelle and Griffith (2003), and performed a sensitivity study (upper limit estimate) of the effects of this rate on the HCN (00^01) population using the value measured by Hasting et al. (1983).

Previous studies (Yelle and Griffith, 2003; Kim et al., 2005) have not considered the relaxation of HCN in collisions with CH_4. We have included this process in our study with the rate coefficient measured by Cannon et al. (1984) of $6.1x10^{-13}$ cm^3s^{-1} at room temperature. These collisions have a significant effect on the population of HCN(00^01) below 600 km. Since this process may act in both directions, exciting and de-exciting HCN(00^01), its proper inclusion requires the non-LTE population of CH_4(0010) level. This population was calculated with the non-LTE model described by García-Comas et al. (2010).

In addition, we have also considered relaxation of the excited HCN levels in self collisions, process 5 in Table 4. This

process is not significant for most of the HCN levels. Only the high energy (20^00, 21^10, 22^00) levels are affected at altitudes above 700 km, where the relative density of HCN becomes larger.

In order to compute the non-LTE populations of the energy levels, a reference atmosphere, including profiles of pressure-temperature and constituents abundances, is needed. Some of these quantities will also be used later, when performing the inversion of the spectra (Sec. 4). We used here a pressure-temperature profile composed from the Titan's atmosphere engineering model of Yelle (1997) and scaled to Huygens Atmospheric Structure Instrument (HASI) measurements (Fulchignoni, 2005) below 480 km. Above that altitude, the HASI results were taken but smoothed and keeping the profile constant above 650~km in order to remove the oscillations thought to be produced by dynamical effects (see Figure 4). The N_2 profile has been taken from the Cassini Gas Chromatograph Mass Spectrometer (GCMS) measurements (Niemann, 2005), and constrained to INMS-Cassini (Yelle et al., 2006) and UVS-Voyager (Vervack et al., 2004) observations above 1000 km (see Figure 4). The CH_4 number density below 1100 km was that retrieved from the same VIMS spectra near 3.3 μm (García-Comas et al., 2011). Above that altitude, the INMS measurements were adopted (see Figure 4). The non-LTE

populations required in the retrieval (Sec. 4) were self-consistently calculated with the retrieved abundances. For the vibrational temperatures shown in Figures 5-9 a mean HCN profile (see Figure 10) was used.

Figure 4

The non-LTE population of a level ν with energy E_ν is usually described in terms of its vibrational temperature:

$$T_v = -\frac{E_v}{k \ln\left(\frac{n_v g_0}{n_0 g_v}\right)},$$

where n_ν and n_0 are the number densities of level ν and of the ground vibrational state, and g_ν and g_0 their respective degeneracies. Figures 5 and 6 show the vibrational temperatures, for the HCN energy levels for SZA=60°, and the collisional rate coefficients listed in Table 4 (the nominal model). The populations of the major contributing levels to the 3.0 μm emission in the Titan's upper atmosphere are discussed below.

Figure 5

Figure 6

3.2 Non-LTE populations and their sensitivity to model parameter uncertainties

From the levels listed in Table 3 there are several transitions emitting in the 3.0 μm (~3300 cm^{-1}) region. The strongest emission takes place through the $00^01 \rightarrow 00^00$ transition. Other weaker bands, as $00^02 \rightarrow 00^01$ and $01^11 \rightarrow 01^10$, also contribute to the Titan's limb emission, although marginally, with values of around 2-6% and 1.5-4%, respectively, at tangent heights of 1100-500 km. Figure 7 shows the contribution to the radiance of all the three transitions plotted versus altitude.

Figure 7

The population of the (00^01) level depends on several parameters, the most important being solar illumination. Figure 8 shows the variation of the vibrational temperature of the (00^01) level with SZA. As we can see, the change is very large because this band is optically thick even at high altitudes and hence, for large SZAs, a large fraction of the solar flux is absorbed at high altitudes, leading to less pumped populations at lower heights. The appropriate SZA of the measurements is included in the calculation of the (00^01) vibrational temperature in the retrieval of HCN.

Figure 8

Figure 9 shows the effects of the HCN VMR on the vibrational temperature of the ($00^0$1) state. Although the ($00^0$1) vibrational temperature is updated in each iteration step of the retrieval (see Sec. 4), we illustrate here its dependence on the HCN abundance. We show this effect by changing the nominal HCN VMR by factors of 10 and 0.1. We see that the effects are altitude dependent. For higher HCN densities, the atmosphere is more opaque and hence the solar flux penetrates less profound, originating smaller populations at lower altitudes, below around 450 km. However, the populations show a different behavior at higher altitudes (above ~600 km): larger populations for larger VMRs. This is a consequence of the optically thick regime of this band around 600-700 km. At these altitudes, where the solar flux is largely absorbed, collisions are not efficient enough to thermalize the solar radiation, and photons are re-absorbed and re-emitted many times before they are thermalized or escape to space. The more optically thick the atmosphere is, the more important the radiative processes are, and then a larger excitation temperature is needed to emit away the absorbed solar radiation. The upwelling radiative flux is larger and, because the excitation temperature at higher altitudes (>800 km) depends on the absorption of the upwelling flux, it leads to higher vibrational temperatures. The same arguments apply for a less abundant HCN atmosphere. Quantitatively, a factor of 10 in the VMR can

lead to a change in the vibrational temperature of as much as 5 K above 600 km, which translates in a change of about 30% in the 3.0 μm emission.

Figure 9

We have performed calculations of the HCN($00^0$1) vibrational temperature by changing the pressure/temperature profile by likely profiles, e.g. those recommended in Yelle's engineering model (Yelle et al., 1997), and found that the vibrational temperatures are smaller than 0.5 K above 400 km.

Concerning systematic errors in the non-LTE model, Figure 10 shows the effects of the uncertainty in the collisional quenching with N_2 and the effect of the CH_4 collisions. Considering the collisional rate with N_2 of Hasting et al. (1983) ($2.6x10^{-14}$ cm^3s^{-1}) instead of that of Yelle and Griffith ($2x10^{-15}$ cm^3s^{-1}) leads to a depletion in the T_v of ($00^0$1) of 1-2 K (6-12% in radiance) between 600 and 800 km and smaller than 1 K above. Below 600 km, the change is much larger but we do not retrieve the HCN abundance in that region. The figure also shows that neglecting the quenching with CH_4, process 4, leads to an increase of the ($00^0$1) T_v of 2-3 K. We should note that Yelle and Griffith did not included collisions with CH_4. Hence, the rate they derived for collisions with N_2 should be even lower if collision with CH_4 were included in their model. We conclude that the errors in the retrieved HCN induced by the uncertainties

in the non-LTE model parameters are about 10% at 600-800 km and about 5% above.

Figure 10

4 Retrieval and Radiative transfer model

Titan's limb atmospheric emission has been simulated with the radiative transfer code Geofit Broad Band (GBB) originally designed for the Earth's atmosphere. This code is the self-standing version of the forward model inside the Geofit Multi-Target Retrieval (GMTR) code (Carlotti et al., 2006), but updated to perform simulations over broad frequency intervals using a line-by-line cross sections computation. The GBB code has been upgraded introducing VIMS characteristics (Field Of View and spectral response), and the option to compute non-LTE radiances as described in Edwards et al. (1993). The code has been validated with the non-LTE computations made with KOPRA (Stiller et al., 2002). GBB can properly represents the ellipsoidal Earth's shape and include diffraction. However, in the simulations of Titan's spectra we have assumed the satellite with spherical shape and have neglected diffraction.

The modified GBB forward model (FM) has been included in a retrieval code that exploits the optimal estimation technique [Rodgers, 2000] and is able to retrieve, simultaneously, the kinetic temperature, the population ratios of

vibrational levels originating the measured radiance, and the VMRs of the contributing atmospheric gases, from VIMS spectra. In our particular case of the 3.0 μm emission, since those three quantities are strongly correlated, we have fixed the kinetic temperature and the population ratios, and retrieved the atmospheric species abundances only.

The retrieval procedure minimizes the cost function through the Gauss Newton iterative procedure. The solution at each iteration is expressed by

$$x_{i-1} = x_i + \left(K^T S_m^{-1} K + S_a^{-1} \right)^{-1} \times \left[K^T S_m^{-1} \vec{n} - S_a^{-1} (x_i - x_a) \right]$$

where x_i is the vector of the solution at iteration i, K is the jacobian matrix containing the derivatives of the observations with respect to the retrieved parameters, S_m is the variance covariance matrix (VCM) of the measurements, x_a and S_a are, respectively, the *a-priori* values of the parameters and their VCMs, and n is a vector containing the differences between the observed and the simulated radiances. To assess the quality of the retrieved VMRs we have used a quantifier, namely the individual information gain q_j, computed for each retrieved VMR value using the following expression:

$$q_j = -\ln_2 \left(\frac{S_{r_j}}{S_{a_j}} \right)$$

where S_{r_j} is the diagonal element of the VCM of the retrieval and S_{a_j} is the diagonal element of the a-priori covariance matrix. This quantifier is not an absolute quantifiers but gives a measure, in terms of binary bits of information, of the 'gain' provided by the measurement with respect to the a-priori knowledge of each retrieved value (Rodgers, 2000). The derivatives of the spectra with respect to the retrieved parameters (the jacobians) have been computed numerically. In order to properly model the narrow line's shape at the low pressures of Titan's upper atmosphere, the spectra have been simulated on a frequency grid of 0.0005 cm^{-1}. The spectra have been convolved with the VIMS spectral response.

Hydrogen cyanide spectroscopic data were taken, as for the computation of the non-LTE populations, from the HITRAN 2008 compilation [Rothman et al. (2009)]. We additionally included other bands in the 3.0 μm region, not listed in the HITRAN compilation, e.g. the $01^{1}1 \rightarrow 01^{1}0$ and $00^{0}2 \rightarrow 00^{0}1$ bands. Their spectroscopic data were taken from the HCN compilation of Harris et al. (2002). In total, in the computation, we have included all the transitions occurring among the ground state and the 9 vibrational excited levels marked with an I in Table 2.

To avoid the underestimation of the computed radiances, a very low threshold for the line's strength ($1x10^{-31}$cm^{-1}/(molecule·cm^{-2}) at 296 K) has been used. The vertical distribution of the vibrational temperatures for all the levels involved in the transitions included in our spectra calculation were pre-computed with the model described in section 3 for a set of SZAs from 0 to 90 at 5 degrees steps. The retrieval of the vertical distribution of HCN VMR has been performed in several steps, using the retrieved HCN VMR to update the vibrational temperatures at the appropriate SZA at each step. In the first iterations a higher threshold for the HCN line's strength was used in order to reduce the CPU time. The reference atmosphere described in Sec. 3.1 was used in the simulation of the spectra. In particular the initial guess profile for HCN (used also as a-priori profile in the retrievals) was taken from Yelle and Griffith (2003) and is plotted in Figure 4. The errors in the a-priori VMR profiles have been set up to 100%. In the upper panel of Figure 11 we report, with a black line, VIMS measured spectrum for cube V1563524168 (Latitude 70ºS and SZA=60.8º), and superimposed in red the simulated spectrum at the final step of the retrieval procedure.

We discussed in section 2.2 that also acetylene and ethane contribute to the limb radiances in the 3.0 μm spectral region. We estimated the C_2H_2 contribution to decrease from

about 30% at 650 km to 20%, 10%, 8%, and 6% at 750, 850, 950 and 1050 km, respectively. Although, as already said in sect. 2.2, the HCN and C_2H_2 emissions are well overlapped at VIMS spectral resolution, we have independent information on HCN and C_2H_2. Therefore we have compensated for the poor knowledge of acetylene VMR and NLTE model by retrieving simultaneously the HCN and C_2H_2 abundances. This approach should also compensate for any contribution of the C_2H_6 3.07 μm band to our spectrum, since its spectrum is completely superimposed to the C_2H_2 spectrum. The a priori acetylene VMR profile, plotted in figure 4, was taken from Lavvas (2008) and we assigned a 100% uncertainty to it. The C_2H_2 ν_3 vibrational temperature was calculated approximately by assuming absorption of solar radiation, collisions with N_2 and spontaneous emission. Therefore, since we haven't developed a proper non-LTE model for C_2H_2, we do not report its retrieved VMR because it is affected by very large systematic errors. However, the contribution from C_2H_2 to the emission is smaller than that of HCN and the inspection of the residual does not show any explicit correlation with both HCN and C_2H_2 spectral signatures. Moreover, since we did not have accurate information about the line intensities of the C_2H_6 band at 3.07 μm and a poor estimate of its spectral position (taken from Seo et al., 2009), we assume that the minor contribution from C_2H_6 (cfr. Section 2.2) can be

accounted for through the estimated C_2H_2 contribution. The bottom panel of Figure 11 shows in red the simulation of Titan spectrum at the final step of the retrieval procedure with superimposed the HCN (green) and C_2H_2+C_2H_6 (blue) emissions for the same data collection reported in Figure 2.

Figure 11

The VMRs were retrieved from all collections using the global fit technique developed by Carlotti (1988) at the same vertical grid composed of 6 altitudes starting from 550 km until 1050 km in 100 km steps. The global fit technique uses a nonlinear least-squares fit procedure to fit simultaneously the whole concentration profile from a complete limb-scanning sequence of spectra. For each collection, the retrieval was performed using the pre-computed vibrational temperatures for the closest SZA. No attempt was made to interpolate them at the SZA of the single spectra. We restricted the analysis to the 22 collections that have a SZA smaller than 80º. This was done in order to avoid potential errors caused by gradients in the vibrational temperatures along the line of sight, which is likely to occur at SZA larger than 80º. The lowest altitude in the retrieval grid contains little information on the HCN abundance because its v_3 band is very optically thick at that altitude. Hence the retrieval of few collections only contributes to the determination of HCN VMR at this altitude (see Figure 12).

5 HCN distribution

We applied the retrieval and radiative transfer model described in Section 4 along with the non-LTE modeling of Section 3 to retrieve the VMRs of HCN in the Titan's upper atmosphere. Using the model atmosphere described in section 3.1, from the VMR profiles we have obtained the HCN number densities at the retrieval altitudes. All the values retrieved from the 22 collection of spectra with SZA<80º, together with the mean and the representative noise errors for single profiles, are shown in Figure 12. We plotted only the data with individual information gain values larger than 0.5. The HCN concentration has a maximum value of $5x10^8$ molecules/cm^3 around 700 km. Then it decreases monotonically with an average scale height of about 170 km, reaching a value of $7x10^7$ molecules/cm^3 at 1050 km. The highest variability of the concentration appears to be between 800 km and 1000 km. This variability is clearly larger than the noise error of the measurements (bars) and than the systematic error induced by the non-LTE model parameters uncertainties (5-10%). It therefore suggests that it is real atmospheric variability.

Figure 12

The retrieved spectra have been taken at different latitudes, at two narrow local time intervals, 13-14 h and 16-18 hours, and distinct SZAs. We then plotted the HCN densities as

function of these variables to find out possible correlations. The plot against latitude did not show a clear pattern, but that versus SZA did show a systematic behavior (see Figure 13). This figure shows that the HCN number density above around 800 km decreases as SZA increases. That is, the HCN increases when/where the atmosphere is less illuminated. The behavior is more clearly seen in Figure 14 that shows the HCN abundance at 950 km as function of SZA distinguishing the two local time intervals. It shows that the HCN concentration is well correlated with SZA, irrespective of the local time. It then suggests that HCN in these regions is in or very close to photochemical equilibrium. This behavior is consistent with the 3D model calculations of Doege et al. (2008), which shows a clear diurnal variation of HCN in the upper atmosphere, with larger values at night. The reason for that is that photo-dissociation of HCN disappears at night leading to higher HCN values. The results shown here should however be taken with caution, since the number of HCN profiles available at the extreme SZAs in Figure 11, 40º and 80º, is very small. A more extensive study of the HCN profiles is then recommend for future studies.

Figure 13

Figure 14

A comparison of our retrieved HCN abundances with previous measurements, both from spacecraft, UVS onboard

Voyager 1 (Vervack et al., 2004) and UVIS onboard Cassini (Shemansky et al., 2005), and from ground-based observations been taken at the Keck II telescope at Mauna Kea (Yelle and Griffith, 2003; Kim et al., 2005), is presented in Figure 15.

Figure 15

We calculated the HCN number densities from Yelle and Griffith (2003) (Y&G hereafter) VMRs using the pressure-temperature reference atmosphere of this work. Our mean profile is generally larger than the UVS and UVIS profiles above around 750 km, although they are close to the lower limit (smaller SZAs) of our VIMS observations. The systematic errors in the UVS and UVIS are, however, rather large, in the order of 100%. Hence, considering the errors in those measurements and the atmospheric variability observed in VIMS, they are in reasonable agreement. An exception is the UVS/Voyager 1 HCN densities below 750 km, which are larger than all other measurements presented here and seems quite anomalous. For UVS ultraviolet occultation measurements the atmospheric scattering at these altitudes is very important and significant errors could be incurred if not accounted properly. This might be a possible reason for the discrepancy. Also, the observation is performed following the star moving through the atmosphere and the different altitudes are not sounded at the same geographical location.

We have also compared with the measurements derived from ground-based observations. As together with a high spectral resolutions they combine a poor spatial resolution, these nadir measurements are mainly sensitive to the atmospheric region around 1 mbar (200-300 km) according to Yelle and Griffith (2003), or 300-600 km as reported by Kim et al. (2005), and are insensitive to the HCN abundance in the thermosphere. Hence, there is a very narrow altitude region were ground-based measurements and VIMS are really comparable (overlap). Then the reason for including such comparison is that they have been extensively used in Titan's studies of the mesosphere and thermosphere and hence it is interesting to see how they compare to the VIMS observations reported here. The comparison shows a good agreement with proposed profile of Yelle and Griffith's in the region above 850 km, falling within the atmospheric variability of VIMS' measurements. Below this altitude, however seems to become slightly smaller. The comparison with the HCN range of values reported by Kim et al. (2005) at these altitudes is at the lower edge of our measurements. It suggests that a better agreement with VIMS observations is achieved for the higher values proposed by Kim et al. (2005).

To verify the coherence of our results with those obtained at lower altitudes we also compared VIMS results to CIRS observations. Figure 16 shows the VIMS VMR profiles together

with those of CIRS as retrieved by Vinatier et al. (2010) below 500 km. The CIRS profiles come from nine sets of limb spectral acquisition taken between February 2005 and May 2008 with vertical resolutions of about 35 km. A better agreement of VIMS mixing ratios is found with those of CIRS taken in the southern hemisphere. This is consistent with the fact that both CIRS and VIMS observations were taken in the same Titan's season, when the southern hemisphere was in the summer. In the other hemisphere, dynamical models predict a winter polar vortex linked to the subsiding branch of the Hadley cell (Hourdin et al., 2005; Achterberg et al., 2008) that would enrich nitriles at stratospheric levels. This fact seems to be confirmed by CIRS observation at 80ºN that see a higher concentration of HCN (Teanby et al., 2007) and does not properly match the VIMS mixing ratios retrieved for the southern hemisphere.

Figure 16

6 Summary and Conclusions

We present in this paper HCN concentrations in the 600 to 1100 km altitude range from VIMS non-LTE emission near 3 μm. These measurements are very important since they come to fill an altitude gap where this species has been very scarcely measured, and where it plays a major role both on the chemistry and energy balance (thermal structure) of this region. The VIMS

daytime spectra have been analyzed and showed that in the altitude of interest here (600-1100 km) the aerosol scattering contribution is negligible. While the daytime emission is high up to tangent heights around 1100 km, the nighttime vanishes at very low altitudes, suggesting that the daytime emission originates under non-LTE conditions. The spectrally integrated radiances near 3.0 μm shows a monotonically decrease with tangent altitude, and a slight increase with solar zenith angle in the 40º-80º interval around 800 km. At larger solar zenith angles (80-100º) the radiances fall off as it is expected from an optically thick band where solar photons are severely absorbed at higher altitudes.

The inversion of VIMS spectra near 3.0 μm have been carried out with an "state-of-the-art" retrieval code, amply used and tested in Earth's atmosphere studies and able to handle non-LTE emissions. A sophisticated non-LTE model of HCN energy levels has also been developed in order to calculate the HCN populations required in the forward model of the retrieval code. The model calculates the non-LTE populations of the 29 energy levels, including those that mainly contribute to Titan's 3.0 μm radiance, the $00^0 1$, $01^0 1$ and $00^0 2$ levels. A detailed and thorough study of the processes and parameters driven the population of the major contributing level, $00^0 1$, has been carried out. This includes its variability with solar illumination, its sensitivity to

the HCN concentration, to the more uncertain collisional parameters deactivating its population (with N_2 and CH_4), and to the likely changes in the pressure temperature profile. The 00^01 population changes significantly with SZA and HCN VMR and hence these dependencies were taken into account in the retrieval. We estimated the errors in the retrieved HCN induced by the uncertainties in the collisional rate coefficients and found to be about 10% at 600-800 km and about 5% above. These are significantly smaller than other error sources, including the instrumental noise.

HCN profiles were retrieved from the 22 spectra collections with SZA smaller than 80º. HCN was retrieved simultaneously with C_2H_2+C_2H_6. The mean HCN concentration retrieved has a maximum value of $5x10^8$ molecules/cm^3 around 700 km and decreases monotonically above with an average scale height of about 170 km, reaching a value of $7x10^7$ molecules/cm^3 at 1050 km. The densities retrieved from the 22 spectra collections show a 1-sigma variability larger than the noise, and hence suggests that they are real changes. The HCN density shows a clear dependency with solar zenith angle, larger HCN for weaker illumination, in the SZA=40-80º interval at altitudes above 800 km. It then suggests that the HCN distribution in these regions is mainly controlled by photochemical processes rather than by dynamics. This behavior

is consistent with the 3D model calculations of Doege et al. (2008), which shows a clear diurnal variation of HCN in the upper atmosphere, with larger values at night produced by the lack of photo-dissociations losses.

A comparison with UVS and UVIS measurements show that these are close to the lower limit (smaller SZAs) of our VIMS observations above 750 km. However, they are in reasonable agreement when considering the UV measurement errors and the atmospheric variability observed in VIMS. We have also compared with HCN ground-based measurements which, although they are few sensitive in the VIMS sounded region due to their poor spatial resolution, they have been extensively used in upper atmospheric studies. The comparison shows a good agreement with the profile reported by Yelle and Griffith (2003) above 850 km, falling within the atmospheric variability of VIMS' measurements, but not below this level where larger concentrations of HCN result from our retrieval. About the comparison to the HCN reported by Kim et al. (2005), VIMS data agree better with the upper values that they proposed.

VIMS data were also compared to those retrieved from CIRS measurements taken in the regions below around 500 km. A good agreement of VIMS mixing ratios was found with those of CIRS taken in its corresponding southern hemisphere. As

expected, the agreement was not so good at the northern winter hemisphere where VIMS data are not available.

About future work, it seems that most important aspect is to extent the analysis of VIMS data to other encounters and cubes, where other latitudes and local times were covered in order to establish a more solid ground for the SZA dependency. Also, the joint retrieval of HCN with C_2H_2 could be improved by calculating more accurate non-LTE populations for the v_3 level of C_2H_2. In this way, VIMS observations could even also produce valuable acetylene measurements.

Acknowledgements

This work has been developed thanks to the financial support of the Italian Space Agency. Special thanks are due to Dr. Gianrico Filacchione IASF-INAF for the support in data calibrations. The IAA team was supported by the Spanish MICINN under projects AYA2008-03498/ESP, CSD2009-00038, and EC FEDER funds. We wish to thank J. Tennyson and C. Hill at University College London for providing HCN spectroscopic data.

References

Achterberg R.K, B.J. Conrath, P.J. Gierasch, F.M. Flasar, C.A. Nixon, 2008. Titan's middle-atmospheric temperatures and

dynamics observed by the Cassini Composite Infrared Spectrometer, Icarus 194, 263–277.

Acton C.H., 1996. Ancillary Data Services of NASA's Navigation and Ancillary Information facility, Planet. Space Sci. 44(1), 65-70.

Arnold G. S. and I. W. M. Smith, 1981. Vibrational relaxation of HCN(001) by the noble gases, O_2, N_2 and CO, J. Chem. Soc. Faraday Trans 2, 77, 861-871,.

Banaszkiewicz M., L. M. Lara, R. Rodrigo, J. J. Lopez-Moreno, and G. J. Molina-Cuberos, 2000. A Coupled Model of Titan's Atmosphere and Ionosphere, Icarus 147, 386–404.

Brown R.H., K. H. Baines, G. Bellucci, J.-P. Bibring, B. J. Buratti, F. Capaccioni, P. Cerroni, R. N. Clark, A. Coradini, D. P. Cruikshank,P. Drossart, V. Formisano, R. Jaumann, Y. Langevin, D. L. Matson,T. B. McCord, V. Mennella, E. Miller, R. M. Nelson, P. D. Nicholson,B. Sicardy And C. Sotin, 2004. The Cassini Visual and Infrared Mapping Spectrometer (VIMS) Investigation, Space Science Reviews 115: 111–168.

Brown R.H., K. H. Baines, G. Bellucci, B. J. Buratti, F. Capaccioni, P. Cerroni, R. N. Clark, A. Coradini, D.P. Cruikshank, P. Drossart, V. Formisano, R. Jaumann, Y. Langevin, D. L. Matson, T.B. McCord, V. Mennella, R.M. Nelson, P.D. Nicholson, B. Sicardy, C. Sotin, N. Baugh, C.A. Griffith, G.B. Hansen, C.A. Hibbitts, T.W. Momary, and M.R. Showalter, 2006. Observations in the Saturn system during approach and orbital insertion with Cassini's visual and infrared mapping spectrometer (VIMS), A&A, 446, 707-716.

Cannon B.D., J.S. Francisco, I.W.M. Smith, 1984. The relaxation of HCN(101) by V-T,R and V-V energy transfer. Chem. Phys. 89(1), 141-150.

Carlotti M., Brizzi G., Papandrea E., Prevedelli M., Ridolfi M., Dinelli B. M., and Magnani L., 2006. GMTR: Two-dimensional multi-target retrieval model for MIPAS-ENVISAT observations, Appl. Opt., 45(4), 716-727.

Carlotti, M., 1988. Global fit approach to the analysis of limb-scanning atmospheric measurements, Appl. Opt., 27, 3250-3254.

Conrath B.J., P. J. Gierasch, E. A. Ustinov, 1998. Thermal Structure and Para Hydrogen Fraction on the Outer Planets from Voyager IRIS Measurements, Icarus, 135, 501–517.

Coustenis A. and B. Bézard, 1995. Titan's Atmosphere from Voyager Infrared Observations, Icarus, 115, 126-140.

Coustenis A., A. Salama, B. Schulz, S. Ott, E. Lellouch, Th. Encrenaz, D. Gautier, and H. Feuchtgruber, 2003. Titan's atmosphere from ISO mid-infrared spectroscopy, Icarus, 161, 383-403.

Cruikshank, D. P., Meyer, A. W., Brown, R. H., Clark, R. N., Jaumann, R., Stephan, K., Hibbitts, C. A., Sandford, S. A., Mastrapa, R. M., Fi- lacchione, G., Ore, C. M. D., Nicholson, P. D., Buratti, B. J., McCord, T. B., Nelson, R. M., Dalton, J. B., Baines, K. H., Matson, D. L., Carbon dioxide on the satellites of Saturn, 2010. Results from the Cassini VIMS investigation and revisions to the VIMS wavelength scale, Icarus, 206, 561-572.

Doege, M. C, Marsh, D.R, Brasseur, G.P, Mueller-Wodarg, I., Tokano, T, Newman, C.E., 2008. A 3-D Chemistry Transport Model for Titan's Thermosphere, AGU Fall Meeting Abstracts, pp. A1336.

Edwards D. P., M. López-Puertas and M. A. López-Valverde, 1993. Non-Local thermodynamic equilibrium studies of the 15 μm bands of CO_2 for atmospheric remote sensing, J. Geophys. Res., 98, 14955-14977.

Filacchione, G., 2006. Calibrazioni a terra e prestazioni in volo di spettrometri ad immagine nel visibile e nel vicino infrarosso per l'esplorazione planetaria (On ground calibrations and in flight performances of VIS-NIR imaging spectrometers for planetary exploration). PhD dissertation, Università degli studi di Napoli Federico II. Available at ftp://ftp.iasfroma.inaf.it/gianrico/phd/Filacchione_PHD_2006.pdf (in Italian),.

Filacchione G., Capaccioni F., McCord T.B., Coradini A., Cerroni P., Bellucci G., Tosi F., D'Aversa E., Formisano V., Brown R.H., Baines K.H., Bibring J.P., Buratti B.J., Clark R.N., Combes M., Cruikshank D.P., Drossart P., Jaumann R., Langevin Y., Matson D.L., Mennella V., Nelson R.M., Nicholson P.D., Sicardy B., 2007. Saturn's icy satellites investigated by Cassini-VIMS I. Full-disk properties: 350–5100 nm reflectance spectra and phase curves, Icarus 186, 2007, 259-290.

Flasar F.M., R. K. Achterberg, B. J. Conrath, P. J. Gierasch, V. G. Kunde, C. A. Nixon, G. L. Bjoraker, D.E. Jennings, P. N. Romani, A. A. Simon-Miller, B. Bezard, A. Coustenis, P. G. J. Irwin, N. A. Teanby, J. Brasunas, J. C. Pearl, M. E. Segura, R. C. Carlson, A. Mamoutkine, P. J. Schinder, A. Barucci, R. Courtin, T. Fouchet, D. Gautier, E. Lellouch, A. Marten, R. Prangé, S. Vinatier, D.F. Strobel, S.B. Calcutt, P.L. Read, F.W. Taylor, N. Bowles, R. E. Samuelson, G. S. Orton, L. J. Spilker, T. C. Owen, J. R. Spencer, M. R. Showalter, C. Ferrari, M. M. Abbas, F. Raulin, S. Edgington, P. Ade, E. H. Wishnow, 2005. Titan's atmospheric temperatures, winds, and composition. Science, 308, 975–978.

Funke, B., Martín-Torres, F.J., López-Puertas, M., Höpfner, M.,Hase, F., López-Valverde, M. A., and García-Comas, M., 2002. A generic non–LTE population model for MIPAS-ENVISAT data analysis, vol. 4, abstracts of the European Geophysical Society, Nice, France, 21–26 April 2002, CD-ROM, ISSN:1029–7006.

García-Comas, M., M. López-Puertas, B. Funke, B.M. Dinelli, M.L. Moriconi, A. Adriani, A. Coradini, A. Molina, 2011. The

analysis of Titan CH_4 3.3 μm upper atmospheric emission as measured by Cassini/VIMS, Icarus, accepted for publication.

Geballe R., S.J. Kim, K.S.Noll, and C.A.Griffith, 2003. High-resolution 3 micron spectroscopy of molecules in the mesosphere and troposphere of Titan, Astrophys. J., 583, L39-L42.

Hanel H., B. Conrath, F. M. Flasar, V. Kunde, W. Maguire, J. Pearl, J. Pirraglia, R. Samuelson, L. Herath, M. Allison, D. Cruikshank, D. Gautier, P. Gierasch, L. Horn, R. Koppany, C. Ponnamperuma, 1981. Infrared Observations of the Saturnian System from Voyager 1, Science 212, 192-200.

Harris G.J., Polyansky O.L., Tennyson J., 2002. Opacity Data for HCN and HNC from a New Ab Initio Line List. Astrophys. J. 578, 657-663.

Hastings P.W., M.K. Osborn, C.M. Sadowski, and I.W.M. Smith, 1983. Vibrational relaxation of HCN(002), J. Chem. Phys., 78 (6), 3893-3898.

Hourdin, F., Lebonnois, S., Luz, D., Rannou, P., 2004. Titan's stratospheric composition driven by condensation and dynamics, J. Geophys. Res. 109, doi:10.1029/ 2004JE002282. E12005.

Kim S.J., T.R. Geballe, K. S. Noll, Regis Courtin, 2005. Clouds, haze, and CH_4, CH_3D, HCN, and C_2H_2 in the atmosphere of Titan probed via 3 μm spectroscopy, Icarus 173, 522-532.

Lavvas P.P., A. Coustenis, I.M. Vardavas, 2008. Coupling photochemistry with haze formation in Titan's atmosphere, Part II: Results and validation with Cassini/ Huygens data, Planet. Space Sci., 56, 67-99.

Liang M.C., Y. L. Yung, D. E. Shemansky, 2007. Photolytically Generated Aerosols in the Mesosphere and Thermosphere of Titan, Astrophys. J., 66,1 L199-L202.

Marten A., T. Hidayat, Y. Biraud, R. Moreno, 2002. New Millimeter Heterodyne Observations of Titan: Vertical Distributions of Nitriles HCN, HC_3N, CH_3CN, and the Isotopic Ratio $^{15}N/^{14}N$ in Its Atmosphere, Icarus 158, 532-544.

McCord T.B., Coradini A., Hibbitts C.A., Capaccioni F., Hansen G.B., Filacchione G., Clark R.N., Cerroni P., Brown R.H., Baines K.H., Bellucci G.,. Bibring J.-P, Buratti B.J., Bussoletti E., Combes M., Cruikshank D.P., Drossart P., Formisano V., Jaumann R., Langevin Y., Matson D.L., Nelson R.M., Nicholson P.D., Sicardy B., Sotin C., 2004. Cassini VIMS observations of the Galilean satellites including the VIMS calibration procedure. Icarus 172, 104-126.

Niemann H.B., S. K. Atreya, S. J. Bauer, G. R. Carignan, J. E. Demick, R. L. Frost, D. Gautier, J. A. Haberman, D. N. Harpold, D. M. Hunten, G. Israel, J. I. Lunine, W. T. Kasprzak, T. C. Owen, M. Paulkovich, F. Raulin, E. Raaen, S. H. Way, 2005. The abundances of constituents of Titan's atmosphere from the GCMS instrument on the Huygens probe, Nature, 438, 779-784.

Rodgers C. D., 2000. Inverse methods for atmospheric sounding: Theory and Practice, Series on Atmospheric, Oceanic and Planetary Physics, vol. 2, World Scientific Publishing Co., Singapore, 65-100.

Rothman, L., Gordon, I.E., Barbe, A. et al., 2009. The HITRAN 2008 molecular spectroscopic database, J. Quant. Spectrosc. Radiat. Transf., 110, 533-572.

Seo H., Kim S. J., Kim, J. H., Geballe T. R., Courtin R., Brown, L.R., 2009. Titan at 3 microns: Newly identified spectral features and an improved analysis of haze opacity, Icarus, 199, 449–457.

Shemansky D.E., A. I. F. Stewart, R. A. West, L. W. Esposito, J.T. Hallett, X. Liu, 2005. The Cassini UVIS Stellar Probe of the Titan Atmosphere, Science 308, 978-982.

Srinivasan N.K., K.S. Gupte, and J.H. Kiefer, 2008. Shock-tube study of relaxation in HCN, J. Chem. Phys. 129(7), 074309.

Stiller G. P., von Clarmann T., Funke B., Glatthor N., Hase F., Höpfner M., and Linden A., 2002. Sensitivity of trace gas abundances retrievals from infrared limb emission spectra to simplifying approximations in radiative transfer modelling, J. Quant. Spectrosc. Rad. Transfer, 72, 249-280.

Strobel D.F. and D.E. Shemansky, 1982. EUV emissions from Titan's upper atmosphere: Voyager 1 encounter, J. Geophys. Res. 87, 1361–1368,.

Teanby N.A., P.G.J. Irwin, R. de Kok, S. Vinatier, B. Bézard, C.A. Nixon, F.M. Flasar, S.B. Calcutt, N.E. Bowles, L. Fletcher, C. Howett, F.W. Taylor, 2007. Vertical profiles of HCN, HC3N, and C2H2 in Titan's atmosphere derived from Cassini/CIRS data, Icarus 186, 364–384.

Teanby N.A., P.G.J. Irwin, R. de Kok, C.A. Nixon, A. Coustenis, E. Royer, S.B. Calcutt, N.E. Bowles, L. Fletcher, C. Howett, F.W. Taylor, 2008. Global and temporal variations in hydrocarbons and nitriles in Titan's stratosphere for northern winter observed by Cassini/CIRS, Icarus, 193, 595–611.

Tobiska W.K, T. Woods, F. Eparvier, R. Viereck, L. Floyd, D. Bouwer, G. Rottman, and O.R. White, 2000. The SOLAR2000 empirical solar irradiance model and forecast tool, J. Atm. Solar Terr. Phys. 62, 1233-1250.

Vervack Jr. R.J., B. R. Sandel, D. F. Strobel, 2004. New perspectives on Titan's upper atmosphere from a reanalysis of the Voyager 1 UVS solar occultations, Icarus 170, 91–112.

Vinatier S., B. Bézard, T. Fouchet, N. A. Teanby, R. de Kok, P. G.J. Irwin, B. J. Conrath, C. A. Nixon, P. N. Romani, F. M. Flasar, A. Coustenis, 2007. Vertical abundance profiles of

hydrocarbons in Titan's atmosphere at 15° S and 80° N retrieved from Cassini/CIRS spectra, Icarus 188, 120–138.

Vinatier, S., Bézard, B., Nixon, C.A., Andrei Mamoutkine A., Carlson, R.C., Jennings, D.E. , Guandique, E.A, Teanby, N.A., Bjoraker, G.L., Flasar, M., Kunde, V.G., 2010. Analysis of Cassini/CIRS limb spectra of Titan acquired during the nominal mission I. Hydrocarbons, nitriles and CO2 vertical mixing ratio profiles. Icarus 205, 559–570

Yelle, R.V., Strobel, D.F., Lellouch, E., Gautier, D., 1997. Engineering models for Titan's atmosphere. In: Huygens Science, Payload, and Mission, ESA SP, Vol. 1177. ESTEC Publications Division, ESTEC, Noordwijk, The Netherlands.

Yelle R.V., C. A. Griffith, 2003. HCN fluorescence on Titan, Icarus 166, 107–115.

Yelle R.V., N. Borggren, V. de la Haye, W.T. Kasprzak, H.B. Niemann,I. Müller-Wodarg , J.H. Waite Jr., 2006. The vertical structure of Titan's upper atmosphere from Cassini Ion Neutral Mass Spectrometer measurements, Icarus 182 567–576.

Waite Jr. J.H., H. Niemann, R. V. Yelle, W. T. Kasprzak, T. E. Cravens, J. G. Luhmann,R. L. McNutt, Wing-Huen Ip, D. Gell, V. De La Haye, I. Müller -Wordag, B. Magee,N. Borggren, S. Ledvina, G. Fletcher, E. Walter, R. Miller, S. Scherer, R. Thorpe, J. Xu, B. Block, K. Arnett, 2005. Ion Neutral Mass Spectrometer Results from the First Flyby of Titan, Science 308, 982-986.

Waite J.H., Jr., D.T. Young, A.J. Coates, F.J. Crary, B.A. Magee, K.E. Mandt, J.H.Westlake, 2008. The source of heavy organics and aerosols in Titan's atmosphere, Proceedings IAU Symposium No. 251, doi: 10.1017/S1743921308021844.

Captions

Figure 1: Limb radiances as measured by VIMS for cube 9485. Here Titan is white-masked to emphasize the atmospheric emission. The South Pole is at the top. Left panel: radiance in the 3.064 mm channel, where HCN has a large contribution..

Lines denote latitude on Titan surface and their correspondence in the atmospheric vertical profiles. Right panel: radiance in the 2.900 μm channel, where no atmospheric molecular spectral feature is present but only scattering contributes to the emission. The altitude levels are shown at steps of 500 km starting from the surface.

Figure 2: VIMS spectra from cube V1563524168 from the collection extracted for the latitude 70ºS and SZA=60.8º (see Table 1) for tangent altitudes ranging from 275 km to 1062 km. The emissions from hydrogen cyanide (HCN) (and C_2H2 at lower altitudes) and methane (CH_4) are shown. The dotted line indicates the noise level of the measurements.

Figure 3: Contour plot of the VIMS radiances integrated between 2.97 and 3.10 μm as a function of altitude and solar zenith angle for the data listed in Table 1.

Figure 4: Reference atmosphere used in this work. Left panel: concentration of nitrogen (red curve), taken from GCMS and methane (cyan triangles) as retrieved from VIMS measurements at 3.3 μm (García-Comas et al., 2011). Right panel: Kinetic temperature (blue curve) and HCN (black solid) and C_2H_2 (dash) volume mixing ratio profiles. The HCN profile was taken from

Yelle and Griffith (2003) and the C_2H_2 from Lavvas et al. (2008). See text for more details.

Figure 5: Vibrational temperatures for the lower energy levels of HCN for daytime conditions (SZA=60º). The curve labeled T_k is the kinetic temperature.

Figure 6: Vibrational temperatures for the higher energy levels of HCN for daytime conditions (SZA=60º). The curve labeled T_k is the kinetic temperature.

Figure 7: Radiance of the strongest HCN transitions contributing to the Titan's limb emission in the 3.0 μm region. The radiances have been integrated in the 2.9-3.1 μm region. The discontinuous curves are related to the single transitions and the solid curve gives the total contribution.

Figure 8: Variation of the vibrational temperature of the ($00^0 1$) level of HCN with solar zenith angle (SZA). T_k is the kinetic temperature. The right panel shows the differences with respect to the T_v for SZA=0º. Note that the curves for SZA=120º and SZA=150º (night) are not shown in the right panel.

Figure 9: Sensitivity of the vibrational temperature of the HCN($00^0$1) level to the HCN volume mixing ratio (vmr) for SZA=60°. T_k is the kinetic temperature. The non-LTE parameters are taken as in the nominal model. The right panel shows the deviations relative to the nominal vmr.

Figure 10: Sensitivity of the vibrational temperature of the HCN($00^0$1) level to the major collisional processes, k_3 and k_4 (see Table 4) for SZA=60°. T_k is the kinetic temperature. Other non-LTE parameters are taken as in the nominal model. The right panel shows the deviations relative to the nominal collisional rates (see Table 3).

Figure 11: Collection of 7 VIMS measured spectra for cube V1563524168 (latitude 70ºS and SZA=60.8º) vertically ordered from the topmost tangent altitude of 1062 km to the lowermost tangent altitude of 527 km. Top panel: the black line is VIMS measured spectrum, superimposed in red is the simulated spectrum at the final step of the retrieval procedure. Bottom panel: the red line is the simulation of VIMS spectra at the final step of the retrieval procedure with superimposed in green the contribution to the simulated spectrum of HCN and in blue the contribution of C_2H_2 and C_2H_6 together.

Figure 12: HCN number density (crosses) retrieved from the 22 spectra profiles with SZA<80º in Table 1. The average HCN profile (diamond and black line) is also shown. The bars represent the mean of the retrieved noise error (representative of the noise error of a single profiles).

Figure 13: Distribution of HCN number density versus altitude and SZA. The retrieved HCN profiles have been binned in SZA boxes 10º wide.

Figure 14: Cross-section of the HCN number density at 950 km as function of SZA. Diamonds are the measurements with local time in the range of 13-14 hours and triangles those taken in the range of 16-18 hours.

Figure 15: HCN number densities as measured by VIMS (this work, diamonds) and spacecraft and ground based measurements. The VIMS profile is the mean of the 22 profiles retrieved (see Table 1). The bars represent the single measurement noise and the shaded area is the 1-sigma atmospheric variability. The HCN range of values from Kim et al. (2005) from their profile in Figure 6 has been plotted showing the two extreme profiles (cross and diamond blue symbols).

Figure 16: VIMS and CIRS HCN volume mixing ratios. CIRS profiles are taken from Vinatier et al. (2010)for latitudes of 20°S (dashed black), 56°S (solid black) and 80°N (solid red). VIMS profiles are shown for the different latitudes and SZAs as listed in the figure. The mean profile (solid thicker black line) as well as a representative single measurement noise error (horizontal bars) are also plotted.

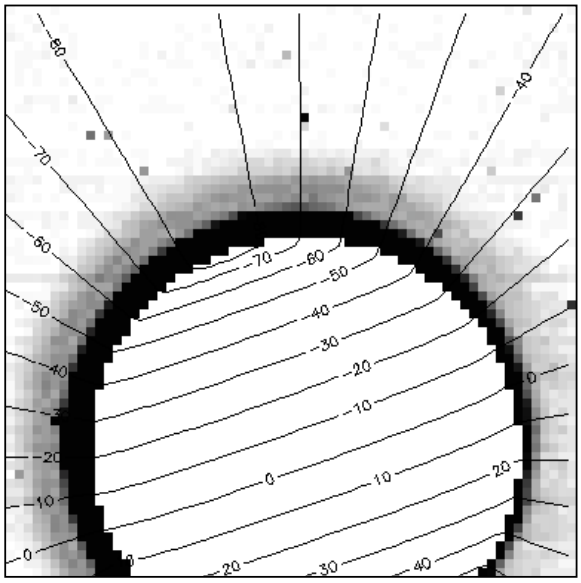

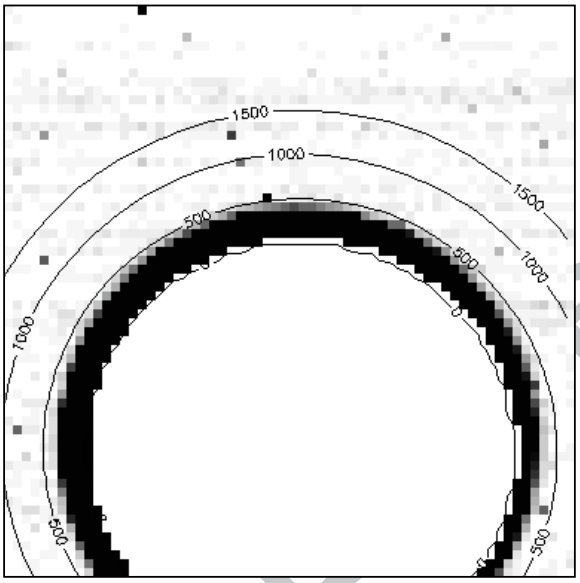

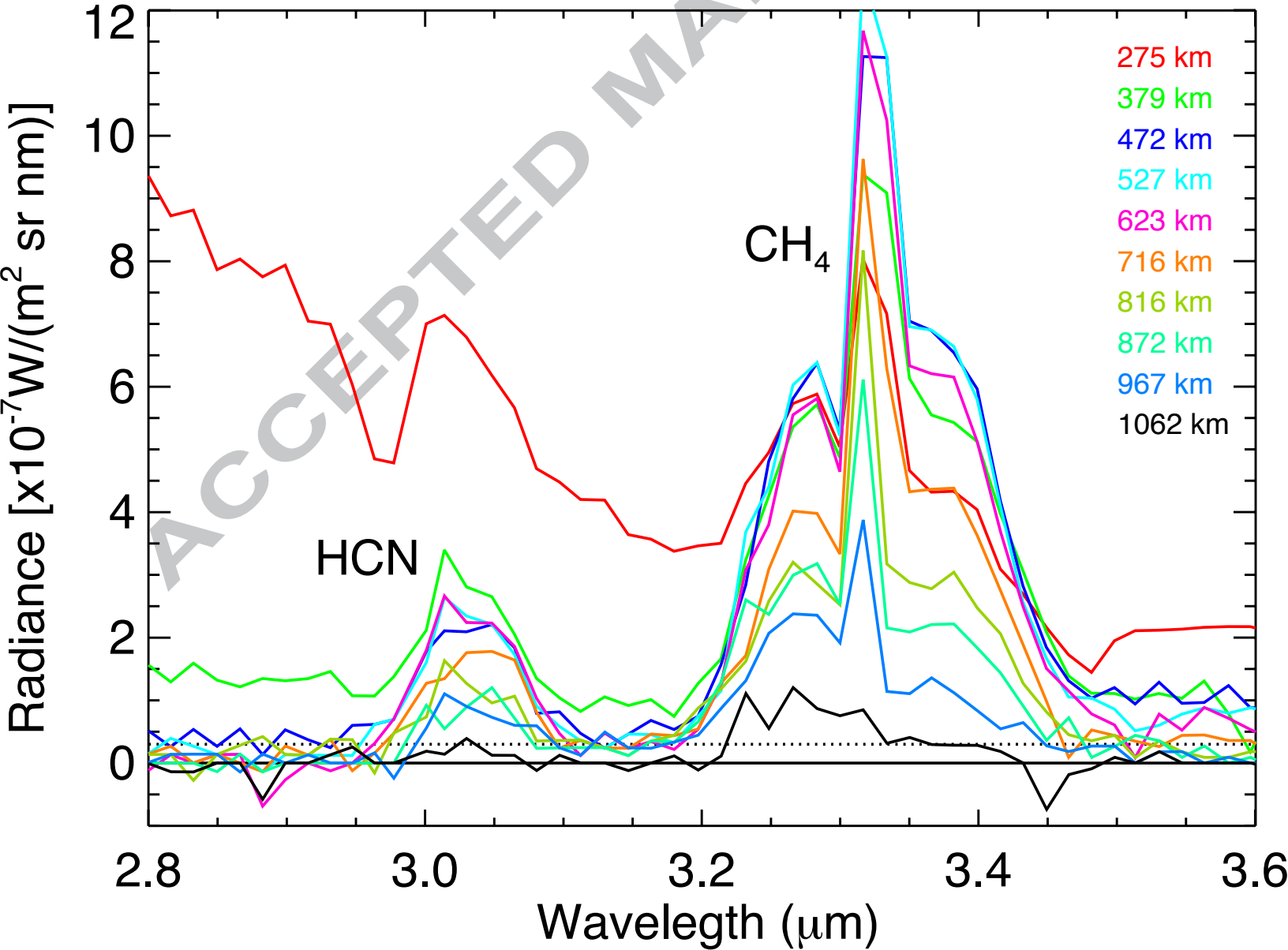

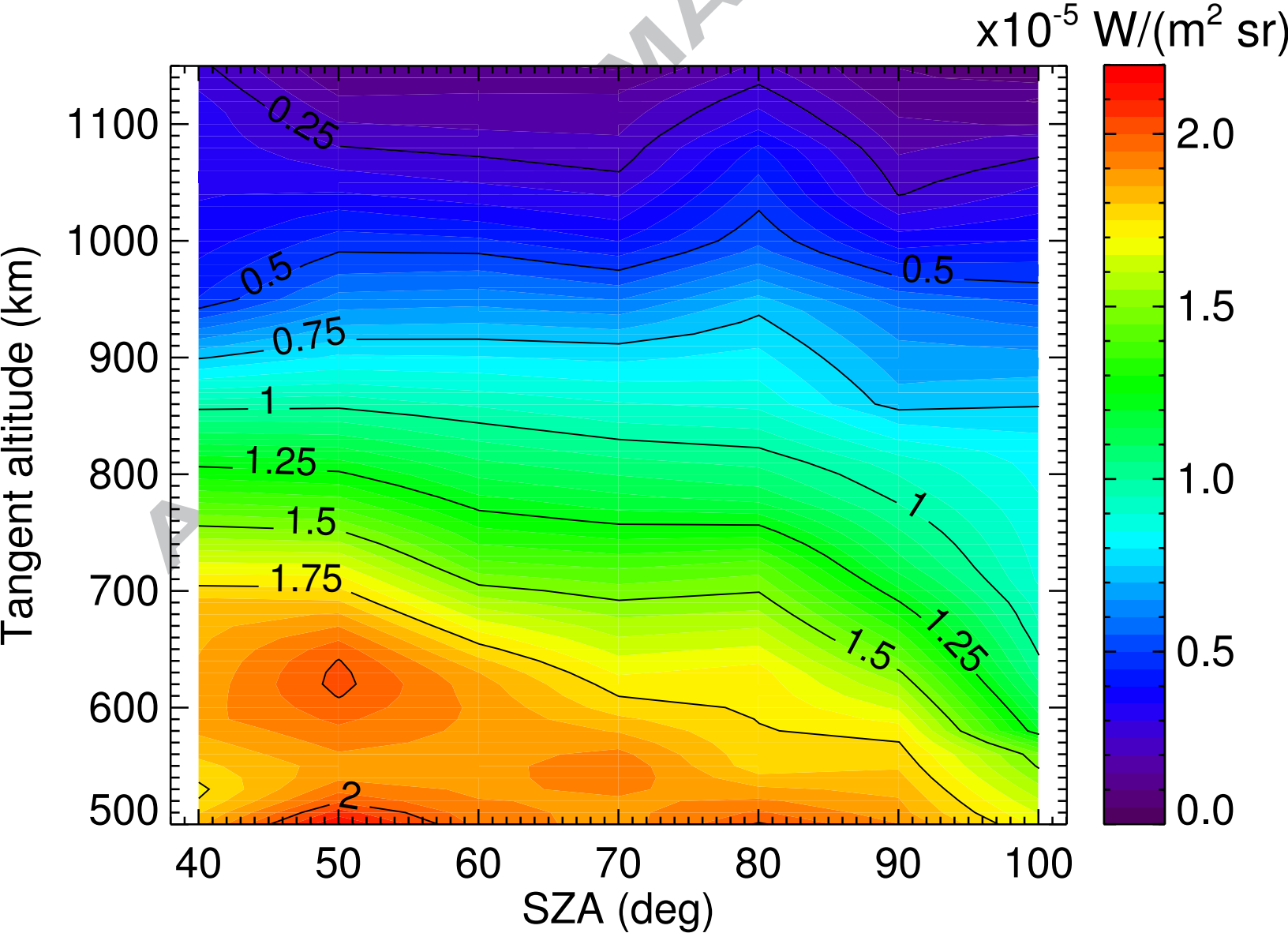

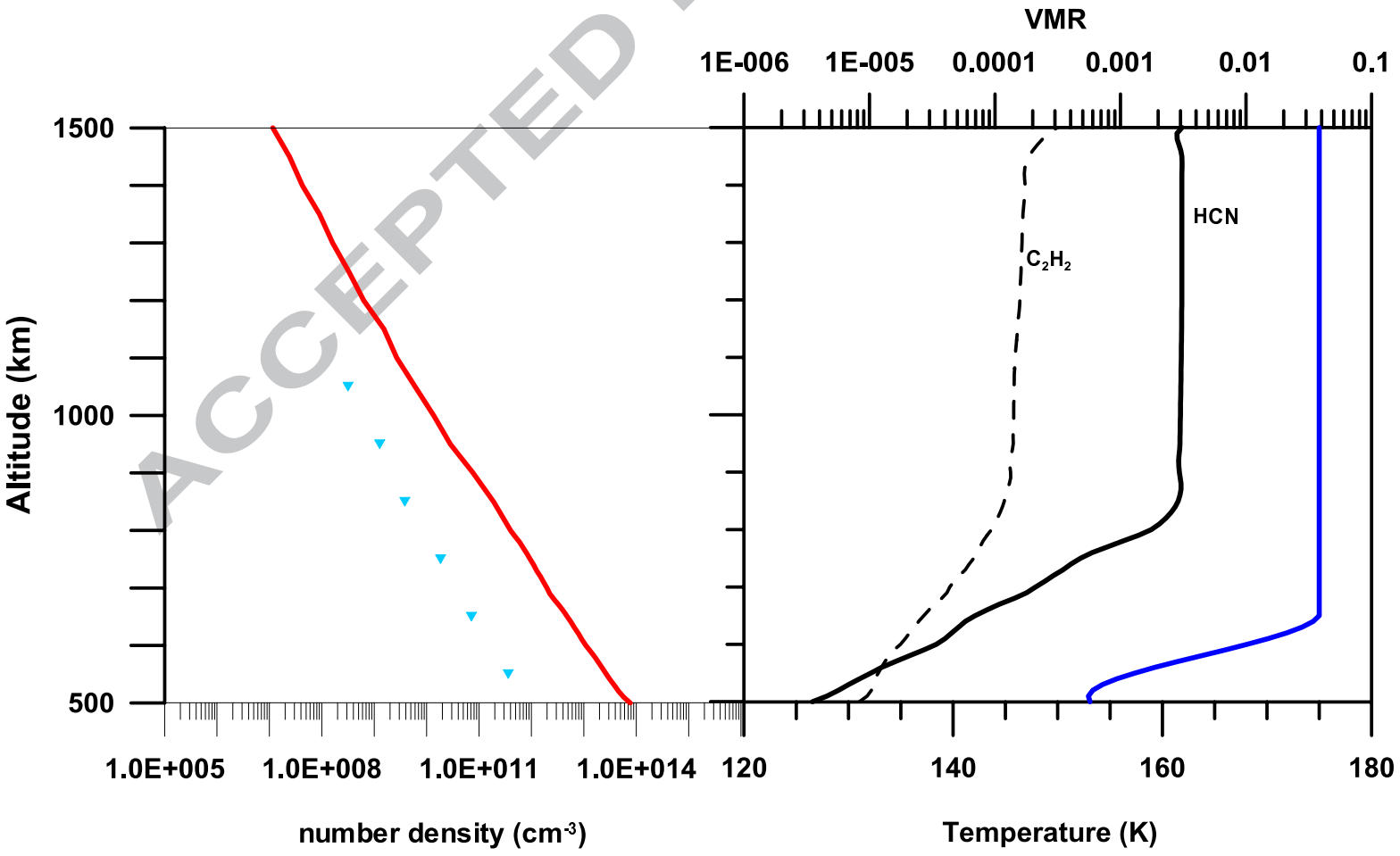

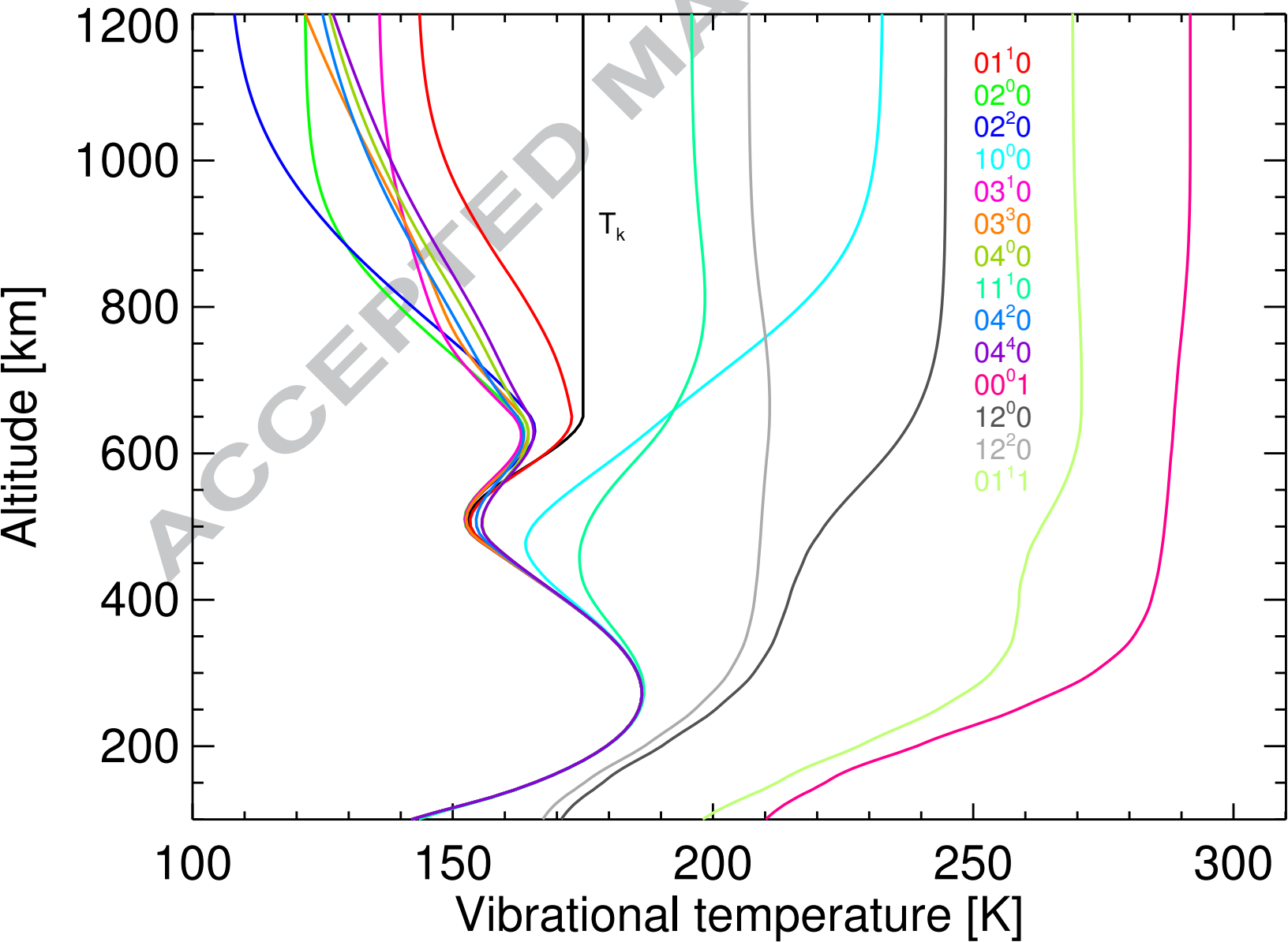

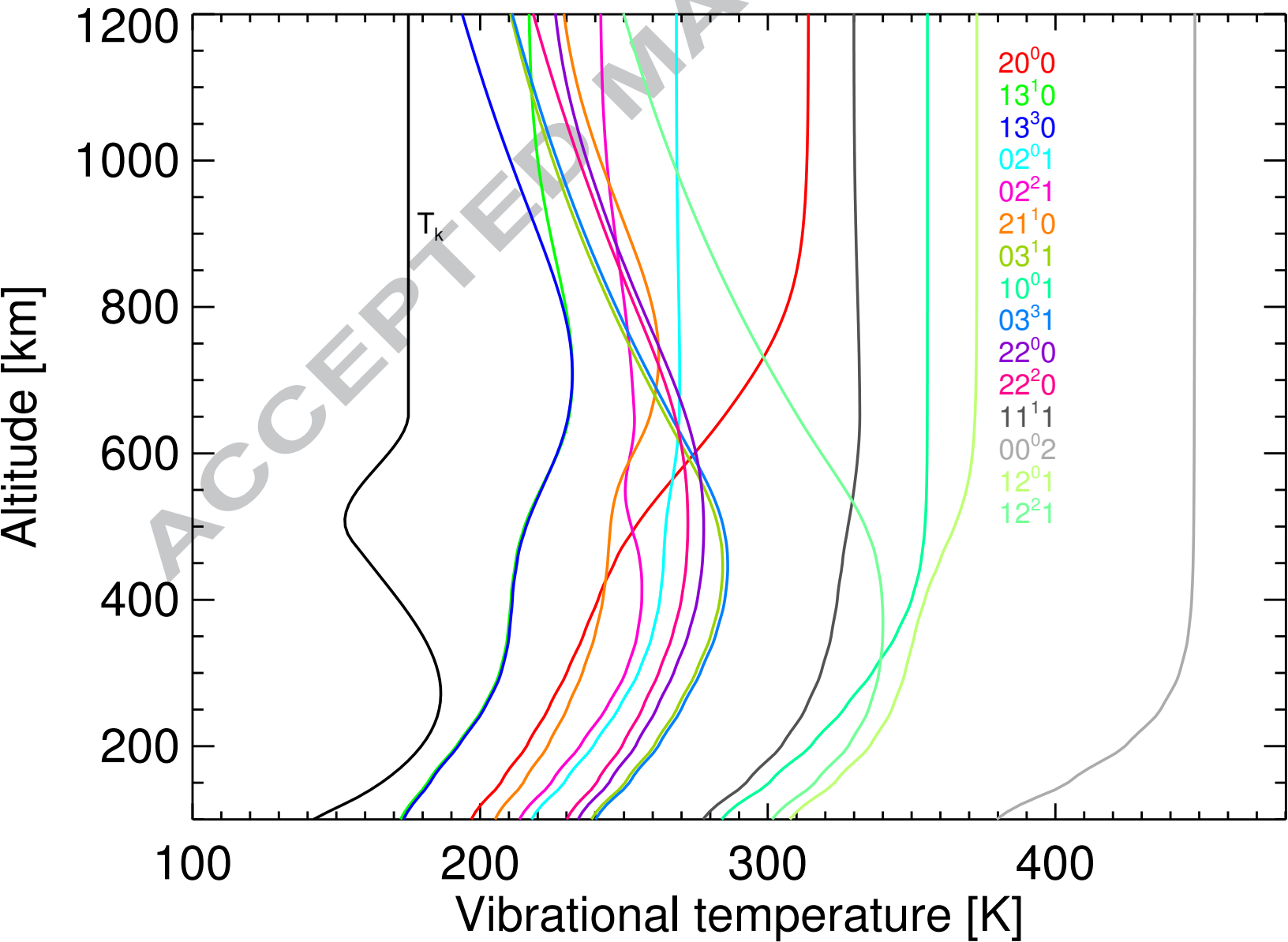

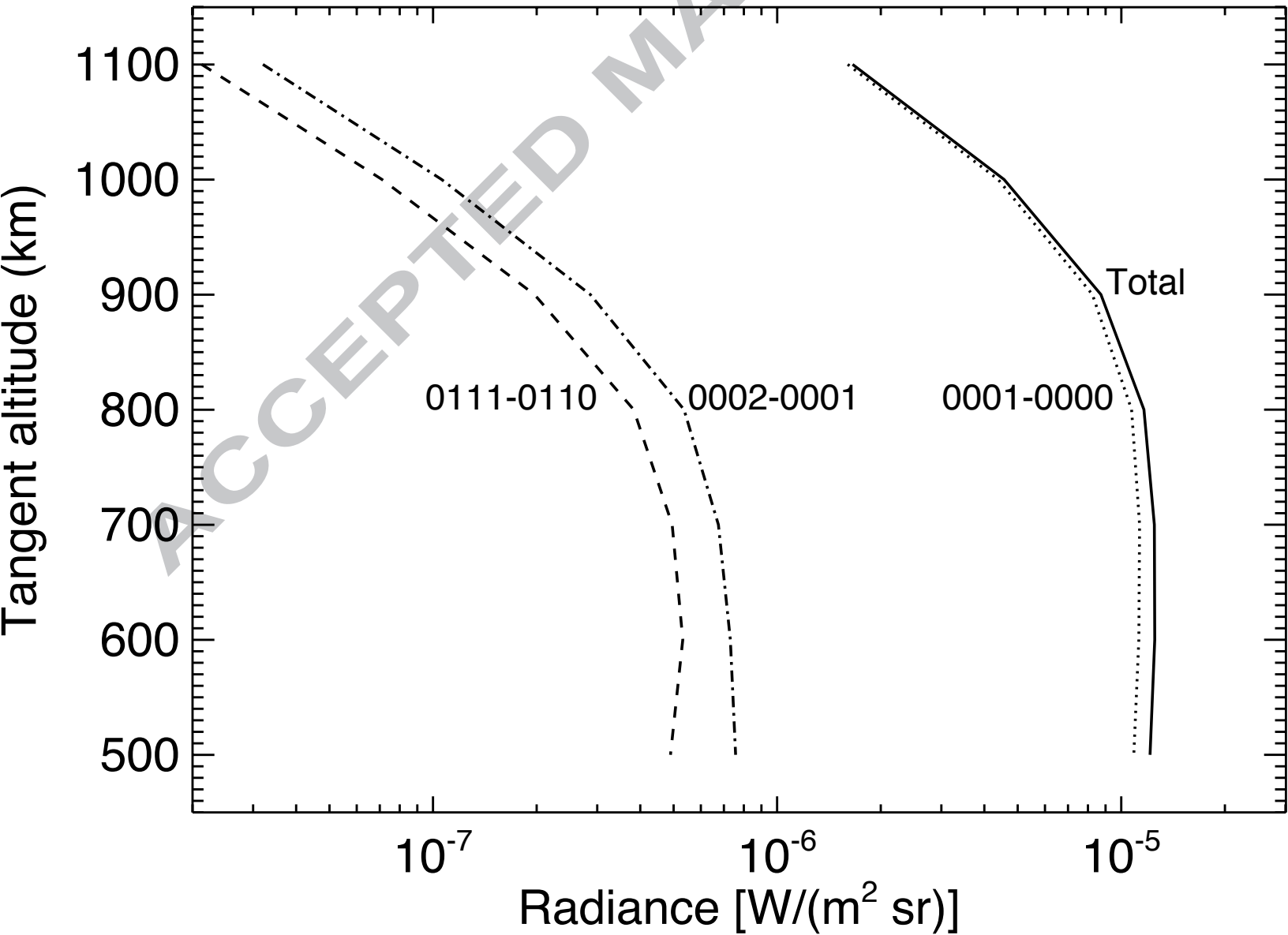

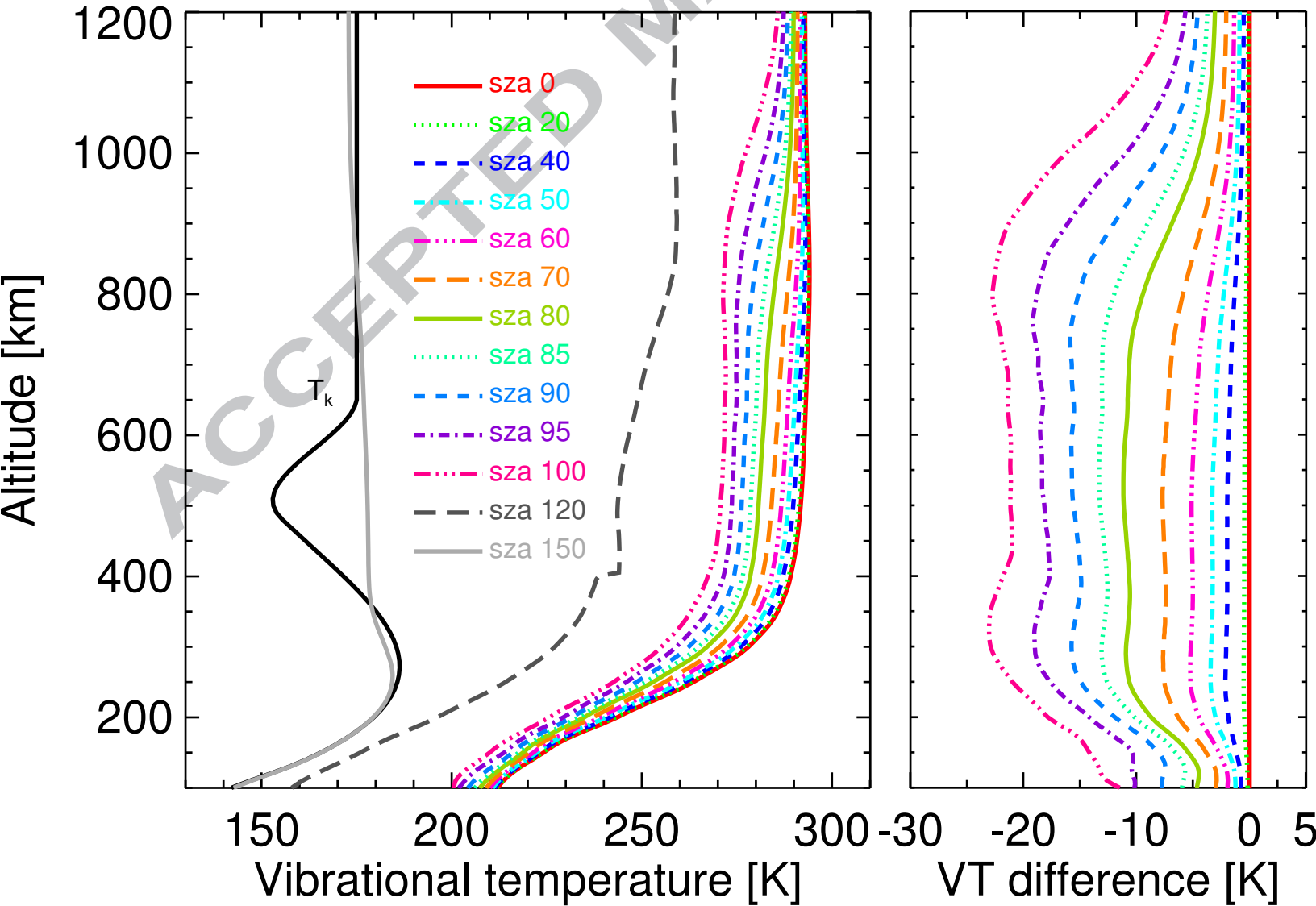

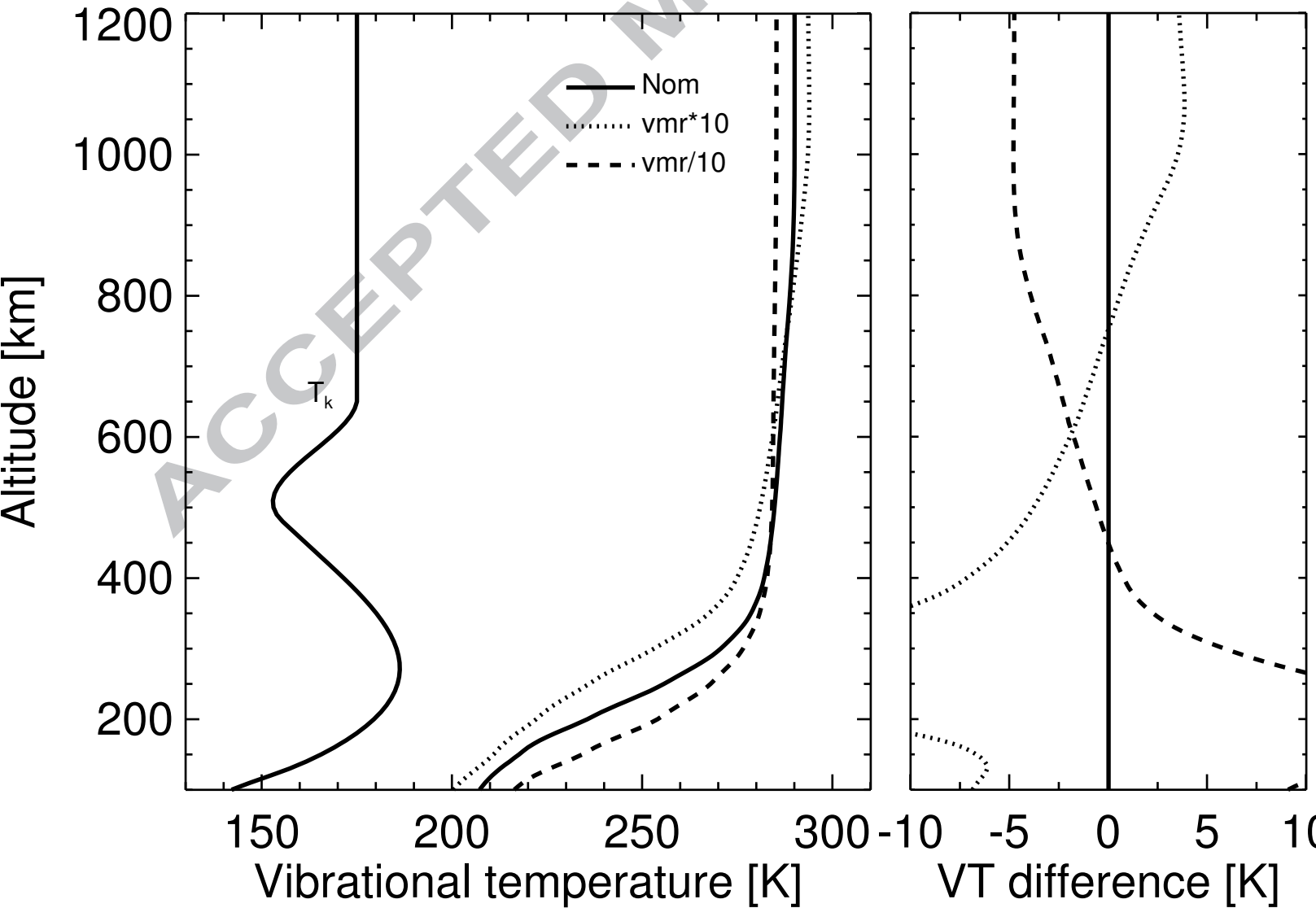

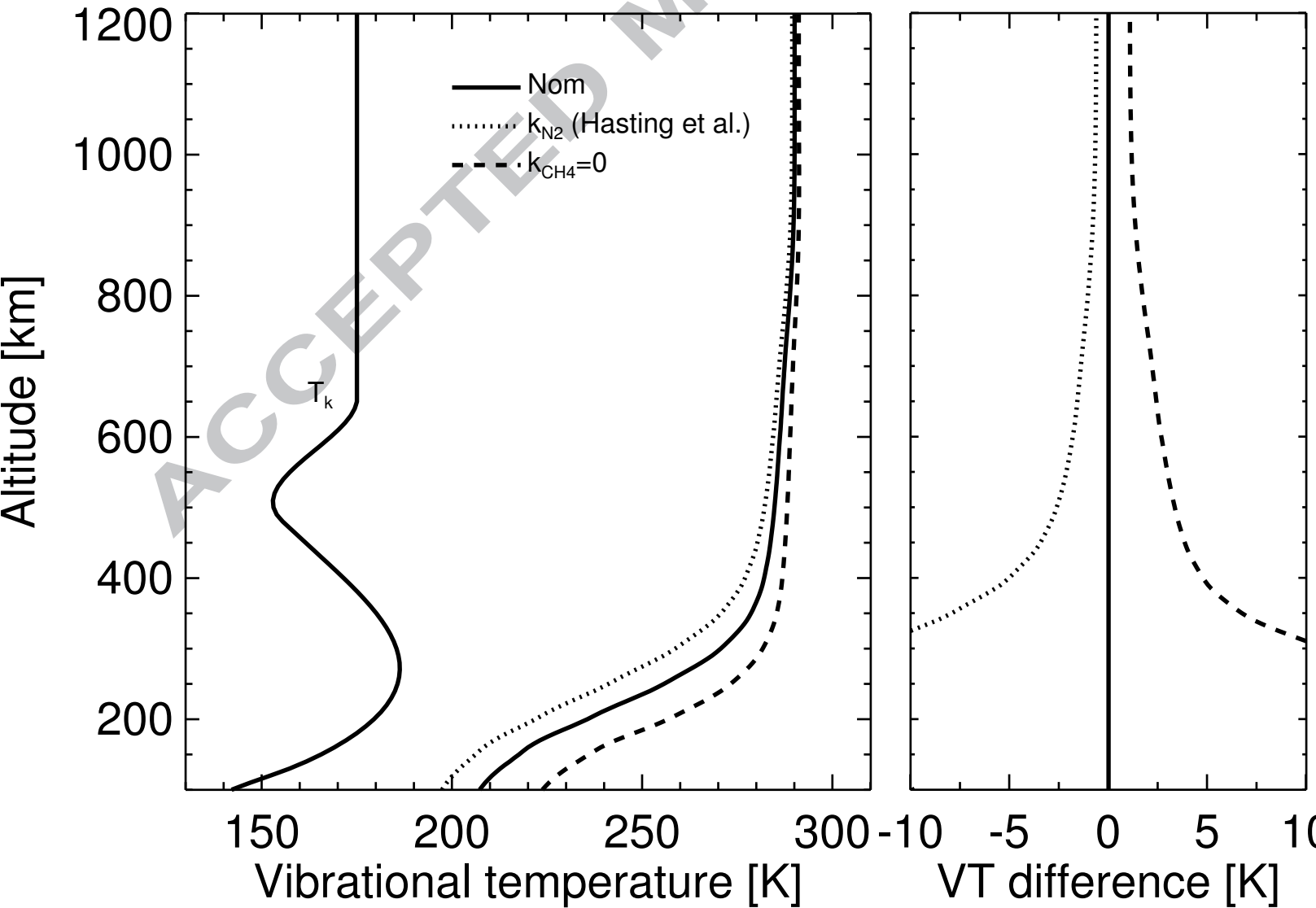

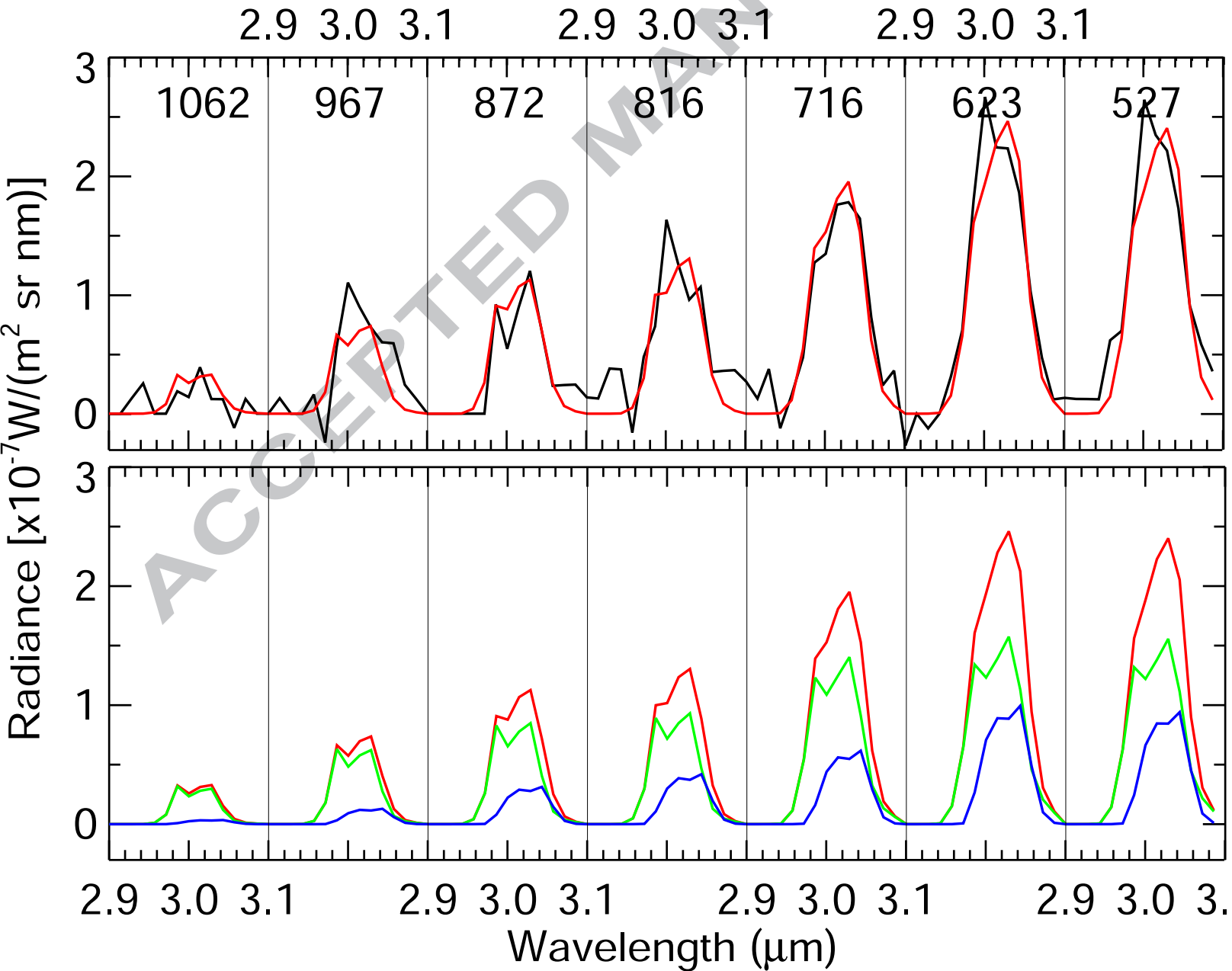

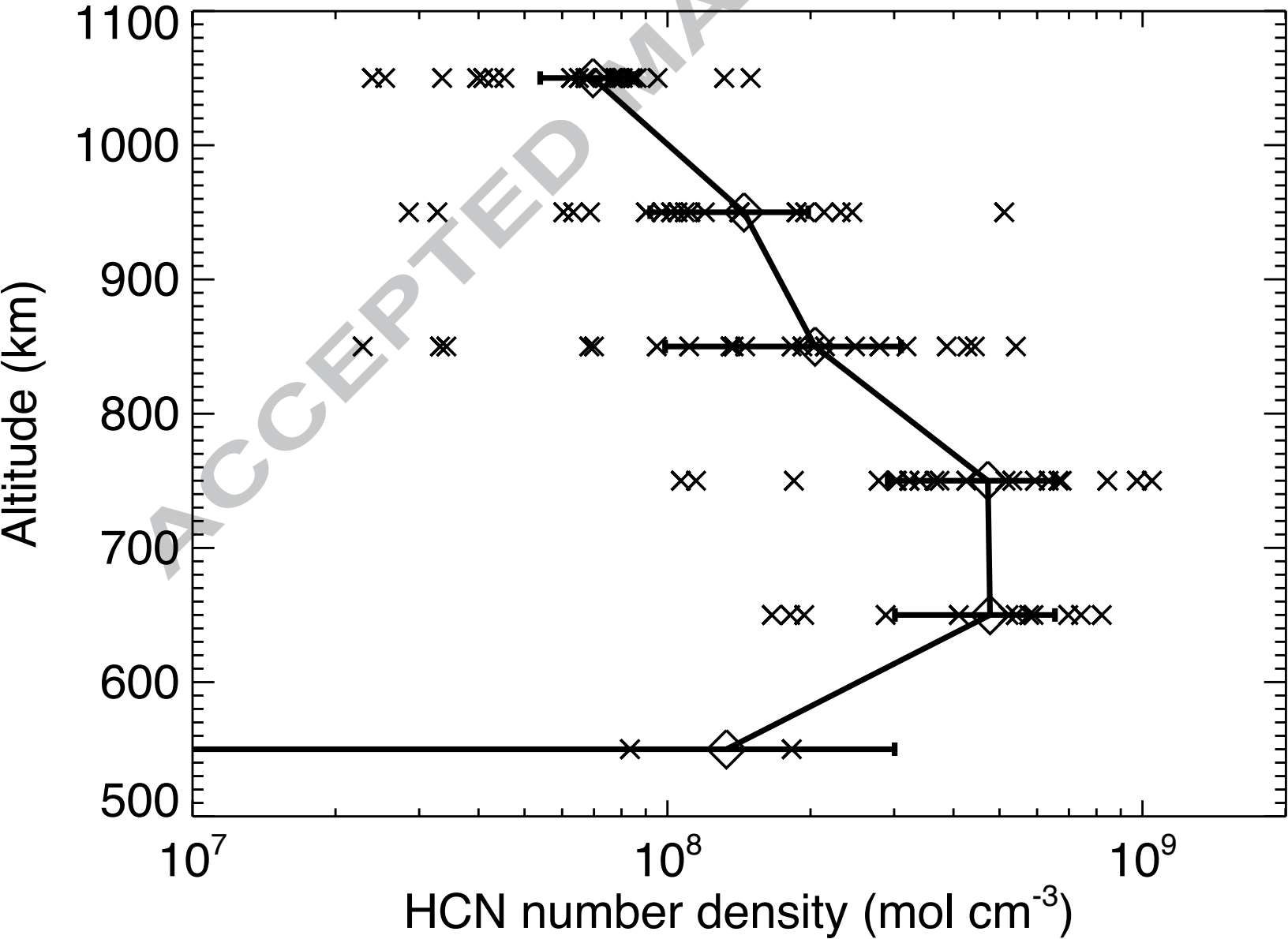

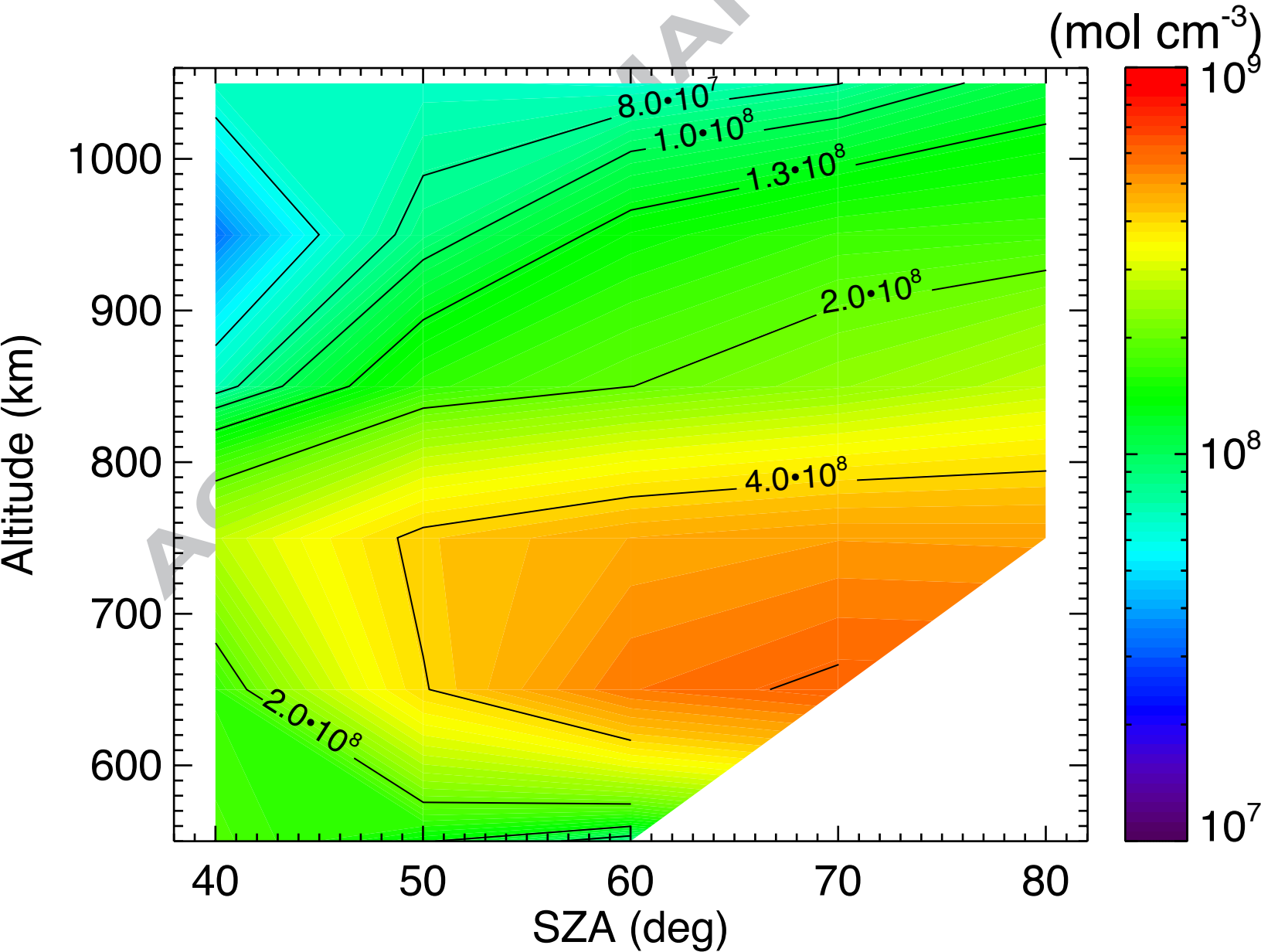

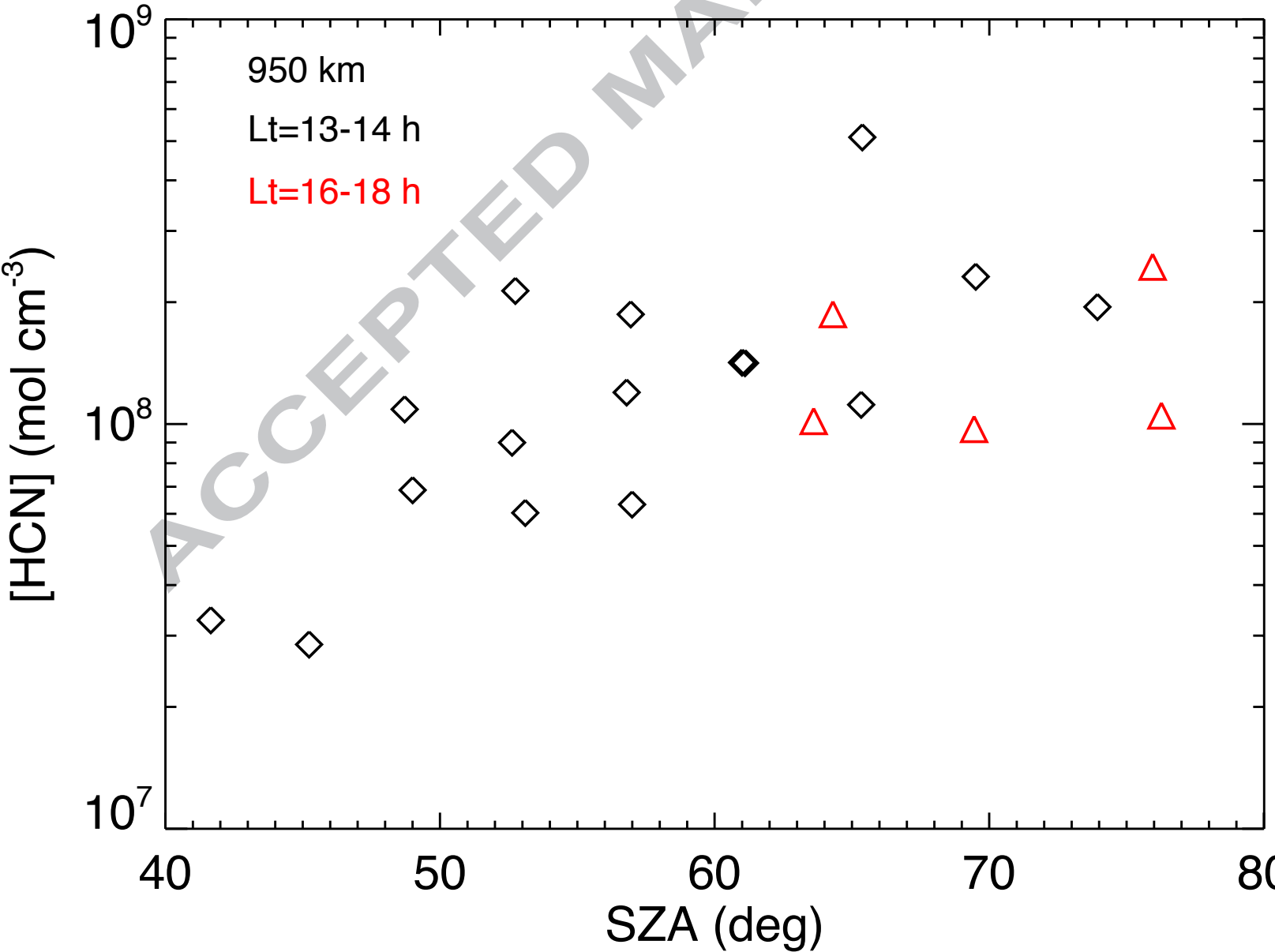

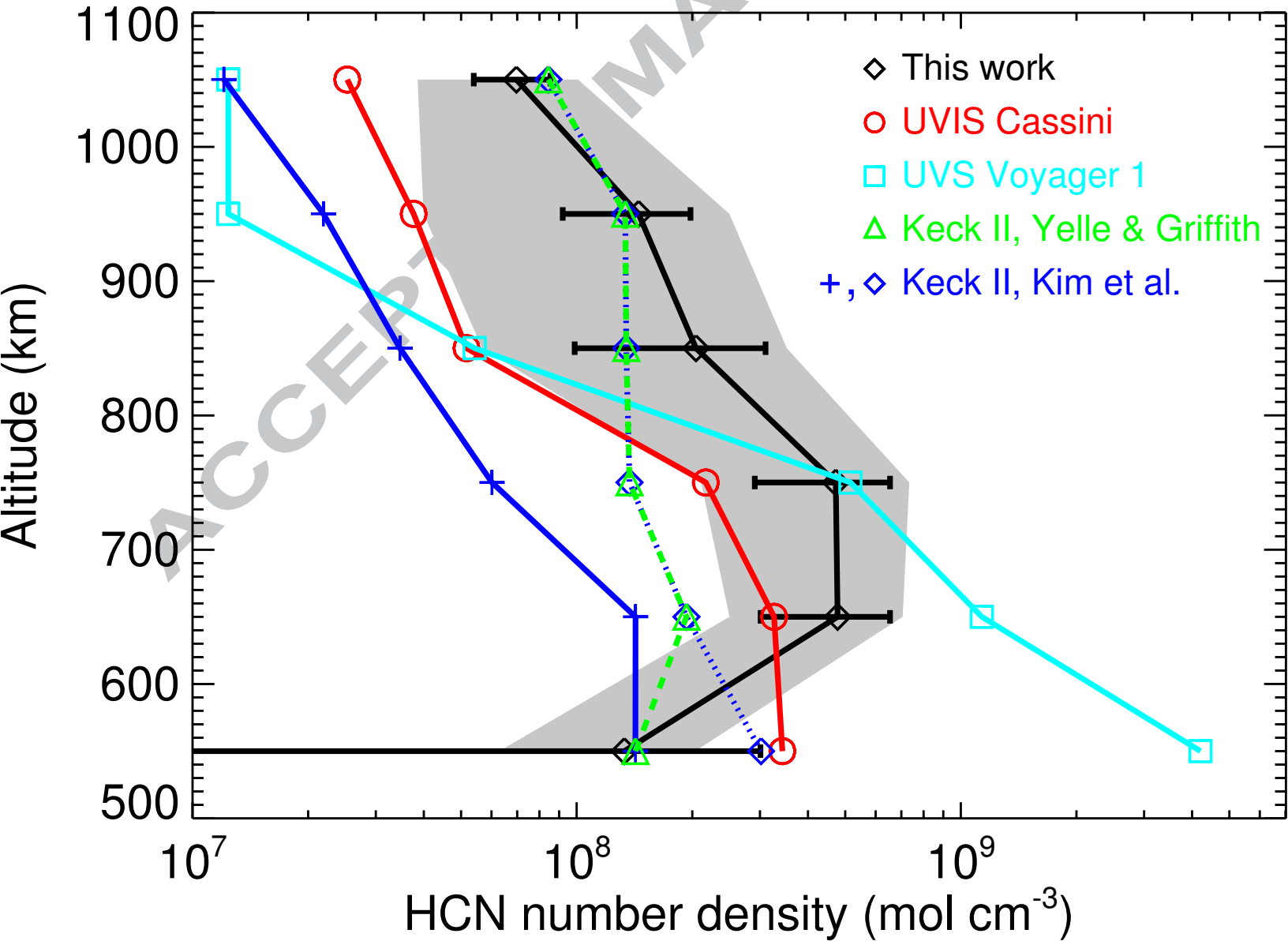

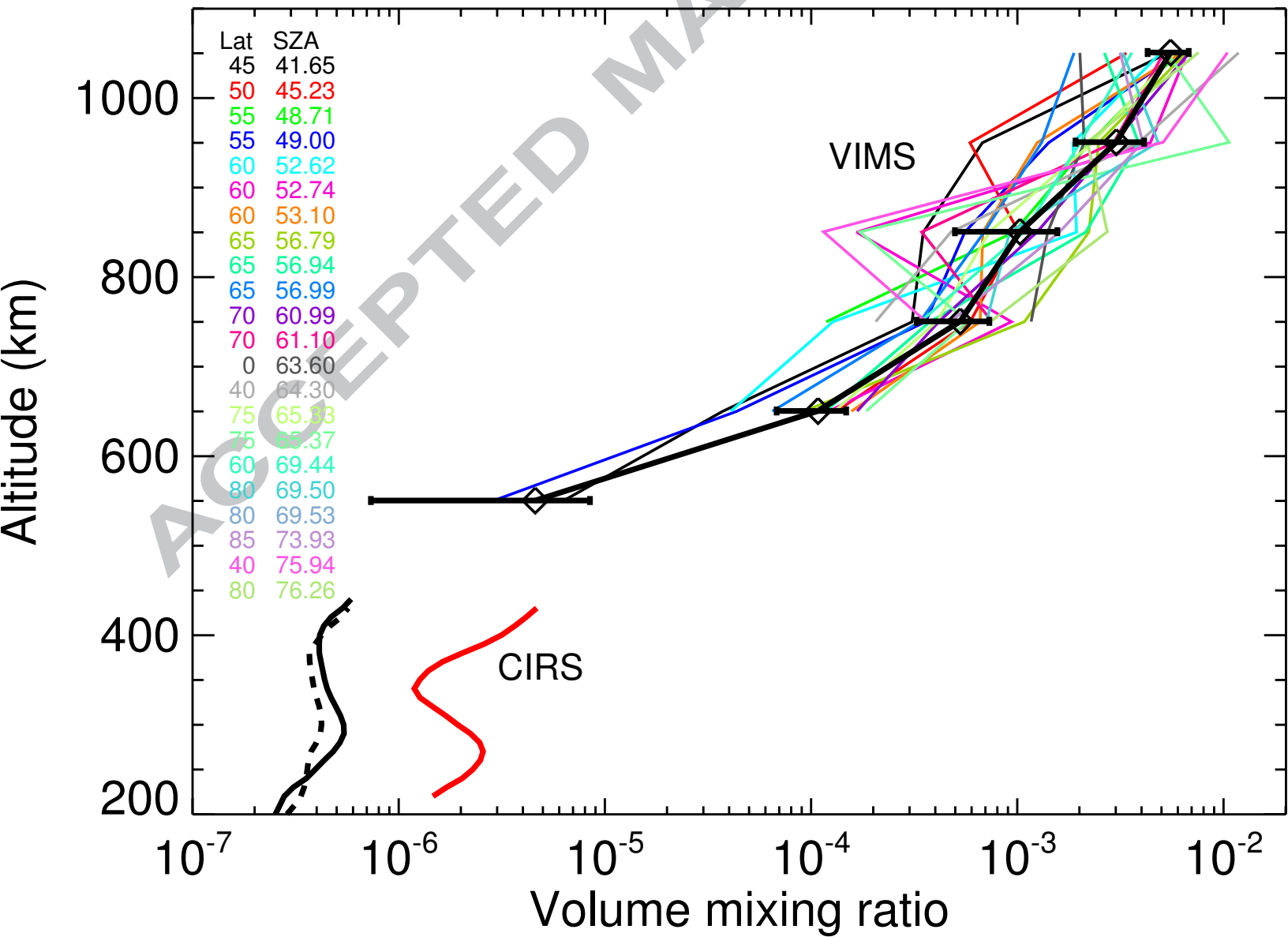

Table 1. VIMS observations analyzed in this work.

Cube name	Flyby	Mean vertical resolution (km)	Phase angle	Latitude(º)	Local Time (hours)	SZA (º)
V1477459118_1	TA	35	13º	40S	18.0	76.1(*)
				0	5.4	99.1
				40N	6.2	102.7
				40N	16.4	87.8
				50N	6.6	102.5
				50N	16.0	90.5
				60N	7.2	101.7
				60N	15.4	92.7
				70N	8.5	100.3
				70N	14.0	95.6
V1563524168_1	T34	22	60º	60S	13.8	53.2(*)
				65S	13.8	57.3(*)
				70S	13.7	60.8(*)
				75S	13.6	65.4(*)
				80S	13.5	69.3(*)
				85S	13.0	73.6(*)
V1563524658_1	T34	22	60º	55S	13.8	49.0(*)
				60S	13.8	52.5(*)
				65S	13.8	56.7(*)
				70S	13.7	61.3(*)
				80S	13.5	69.1(*)
V1563525149_1	T34	22	60º	45S	13.9	41.8(*)
				50S	13.9	45.7(*)
				55S	13.8	49.1(*)
				60S	13.8	53.4(*)
				65S	13.8	57.0(*)
				70S	13.8	60.9(*)
V1567269485_1	T35	37	26º	0	16.2	63.9(*)
				40S	16.3	64.5(*)
				60S	16.5	69.6(*)
				80S	16.8	76.2(*)
				60S	4.1	93.8
				50S	4.2	98.7

(*) Collections used in the retrieval of HCN

Table 2. HCN energy levels for which vibrational temperatures are calculated.

No.	HITRAN ID	FM inclusion	Level(∗)	Energy (cm^{-1})
1	2	I	01^10	713.459
2	3	I	02^00	1411.41
3	4	I	02^20	1427.63
4	5		10^00	2096.85
5	6		03^10	2113.41
6	7		03^30	2144.93
7	9		04^00	2797.97
8	8		11^10	2806.18
9	10		04^20	2814.14
10	44	I	04^40	2862.65
11	14	I	00^01	3311.48
12	11		12^00	3500.92
13	12		12^20	3517.10
14	19	I	01^11	4005.63
15	13		20^00	4173.03
16	16		13^10	4197.26
17	17		13^30	4229.60
18	25	I	02^01	4684.11
19	26	I	02^21	4699.80
20	18		21^10	4878.41
21	30		03^11	5364.71
22	27		10^01	5393.76
23	31		03^31	5397.06
24	22		22^00	5569.20
25	23		22^20	5585.37
26	32		11^11	6083.42
27	38	I	00^02	6519.60
28	36		12^01	6758.49
29	37		12^21	6774.66

(∗) We use the notation of v_3=1 for the H-C bond stretching mode.

Table 3: HCN vibrational bands included in the model.

Group	Upper level*		Lower level*		$\tilde{\nu}_0$ (cm^{-1})	$A^{\dagger}$ (s^{-1})	RT‡
ν_2	$03^{1}1$	(30)	$02^{2}1$	(26)	664.914	1.631	–
	$04^{2}0$	(10)	$03^{3}0$	(7)	669.210	3.600	–
	$12^{0}1$	(36)	$11^{1}1$	(32)	675.061	1.872	–
	$02^{0}1$	(25)	$01^{1}1$	(19)	678.477	3.314	–
	$13^{1}0$	(16)	$12^{2}0$	(12)	680.162	1.631	–
	$03^{1}1$	(30)	$02^{0}1$	(25)	680.608	3.616	–
	$04^{0}0$	(9)	$03^{1}0$	(6)	684.561	7.200	–
	$03^{1}0$	(6)	$02^{2}0$	(4)	685.778	1.631	–
	$11^{1}1$	(32)	$10^{0}1$	(27)	689.663	1.872	–
	$22^{0}0$	(22)	$21^{1}0$	(18)	690.794	3.314	–
	$12^{2}1$	(37)	$11^{1}1$	(32)	691.232	1.872	–
	$01^{1}1$	(19)	$00^{0}1$	(14)	694.152	1.872	–
	$02^{2}1$	(26)	$01^{1}1$	(19)	694.171	3.763	–
	$12^{0}0$	(11)	$11^{1}0$	(8)	694.747	3.314	–
	$13^{1}0$	(16)	$12^{0}0$	(11)	696.333	3.616	–
	$03^{3}1$	(31)	$02^{2}1$	(26)	697.256	5.975	–
	$02^{0}0$	(3)	$01^{1}0$	(2)	697.954	3.314	–
	$04^{2}0$	(10)	$03^{1}0$	(6)	700.732	3.600	–
	$03^{1}0$	(6)	$02^{0}0$	(3)	701.995	3.616	–
	$21^{1}0$	(18)	$20^{0}0$	(13)	705.379	1.872	–
	$22^{2}0$	(23)	$21^{1}0$	(18)	706.966	3.763	–
	$11^{1}0$	(8)	$10^{0}0$	(5)	709.332	1.800	–
	$12^{2}0$	(12)	$11^{1}0$	(8)	710.918	3.700	–
	$13^{3}0$	(17)	$12^{2}0$	(12)	712.504	5.975	–
	$01^{1}0$	(2)	$00^{0}0$	(1)	713.459	1.872	RT
	$02^{2}0$	(4)	$01^{1}0$	(2)	714.171	3.763	–
	$03^{3}0$	(7)	$02^{2}0$	(4)	717.300	5.975	–
	$04^{4}0$	(44)	$03^{3}0$	(7)	717.724	7.200	–
$2\nu_2$	$03^{1}1$	(30)	$01^{1}1$	(19)	1359.085	3.450	–
	$12^{0}1$	(36)	$10^{0}1$	(27)	1364.724	1.989	–
	$02^{0}1$	(25)	$00^{0}1$	(14)	1372.628	1.989	–
	$04^{0}0$	(9)	$02^{0}0$	(3)	1386.556	4.000	–
	$13^{1}0$	(16)	$11^{1}0$	(8)	1391.080	3.450	–
	$22^{0}0$	(22)	$20^{0}0$	(13)	1396.174	1.989	–
	$03^{1}0$	(6)	$01^{1}0$	(2)	1399.949	3.450	–
	$04^{2}0$	(10)	$02^{0}0$	(3)	1402.727	4.000	–
	$12^{0}0$	(11)	$10^{0}0$	(5)	1404.079	1.989	–
	$02^{0}0$	(3)	$00^{0}0$	(1)	1411.413	1.989	–

* Numbers in parenthesis are the ID number in the HITRAN compilation. † Einstein coefficient at 296 K. ‡ Radiative transfer. RT: full radiative transfer among atmospheric layers is included. Sun: The absorption of solar radiation in this band is significant.

Table 4. Collisional processes included in the nominal HCN model.

No.	Process	Rate coefficient (cm^3s^{-1})	Reference
1	$HCN(v_1,v_2,v_3)+N_2 \rightarrow HCN(v_1,v_2-1,v_3)+N_2$	10^{-12}	Srinivasan et al. (2008) rate for Kr and scaled with $k(N_2)/k(Kr)=0.3$ from Arnold and Smith (1981).
2	$HCN(v_1,v_2,v_3)+N_2 \rightarrow HCN(v_1-1,v_2+3,v_3)+N_2$	2.7×10^{-14}	Srinivasan et al. (2008) rate for Kr and scaled with $k(N_2)/k(Kr)=0.3$ from Arnold and Smith (1981).
3	$HCN(v_1,v_2,v_3)+N_2 \rightarrow HCN(v_1+1,v_2+2,v_3-1)+N_2$	2.0×10^{-15}	Yelle and Griffith (2003)
4	$HCN(v_1,v_2,v_3)+CH_4 \Leftrightarrow HCN(v_1,v_2,v_3-1)+CH_4(0010)$	6.1×10^{-13}	Cannon et al. (1984)
5	$HCN(v_1,v_2,v_3)+HCN \Leftrightarrow HCN(v_1+1,v_2+1,v_3-1+HCN(010)$	2.4×10^{-12}	Hasting et al. (1983)

- We present the first concentration retrieval of HCN by Cassini-VIMS limb observations of the Titan upper atmosphere in the altitude range 600-1100 km
- HCN is thought to play an important role in the chemistry and in determining the thermal structure of Titan's thermosphere
- A model for non-LTE HCN emission in Titan atmospheric condition has been developed for the purpose